Hippocampome.org v2.0: a knowledge base enabling data-driven spiking neural network simulations of rodent hippocampal circuits

Diek W. Wheeler[1,3], Jeffrey D. Kopsick[1,2], Nate Sutton[1,3], Carolina Tecuatl[1,3], Alexander O. Komendantov[1,3], Kasturi Nadella[1,3], Giorgio A. Ascoli[1,2,3*]

[1]Center for Neural Informatics, Structures, & Plasticity; Krasnow Institute for Advanced Study; George Mason University, Fairfax, VA, USA
[2]Interdisciplinary Program in Neuroscience; College of Science; George Mason University, Fairfax, VA, USA
[3]Bioengineering Department and Center for Neural Informatics, Structures, & Plasticity; College of Engineering and Computing; George Mason University, Fairfax, VA, USA
[*]Correspondence: ascoli@gmu.edu

Abstract

Hippocampome.org is a mature open-access knowledge base of the rodent hippocampal formation focusing on neuron types and their properties. Hippocampome.org v1.0 established a foundational classification system identifying 122 hippocampal neuron types based on their axonal and dendritic morphologies, main neurotransmitter, membrane biophysics, and molecular expression. Releases v1.1 through v1.12 furthered the aggregation of literature-mined data, including among others neuron counts, spiking patterns, synaptic physiology, *in vivo* firing phases, and connection probabilities. Those additional properties increased the online information content of this public resource over 100-fold, enabling numerous independent discoveries by the scientific community. Hippocampome.org v2.0, introduced here, besides incorporating over 50 new neuron types, now recenters its focus on extending the functionality to build real-scale, biologically detailed, data-driven computational simulations. In all cases, the freely downloadable model parameters are directly linked to the specific peer-reviewed empirical evidence from which they were derived. Possible research applications include quantitative, multiscale analyses of circuit connectivity and spiking neural network simulations of activity dynamics. These advances can help generate precise, experimentally testable hypotheses and shed light on the neural mechanisms underlying associative memory and spatial navigation.

Introduction

Neuroscience knowledge continues to increase every year (Eke et al., 2022; Yeung et al., 2017), making it challenging for researchers to keep abreast of mounting data and evolving information even in their own domain of expertise. Large-scale endeavors, such as the Brain Research through Advancing Innovative Neurotechnologies (BRAIN) Initiative (Insel et al., 2013) and the European Union's Human Brain Project (Amunts et al., 2016), are contributing to this tremendous growth along with the 'long tail' of independent labs and individual scientists (Ferguson et al., 2014). A key organizing principle for neuroscience knowledge is the seminal notion of neuron types (Petilla Interneuron Nomenclature Group et al., 2008; Zeng and Sanes, 2017), which constitute the conceptual 'parts list' of functional circuits. The National Institutes of Health launched the BRAIN Initiative Cell Census Network (BICCN) to help establish a comprehensive reference of the cell type diversity in the human, mouse, and non-human primate brains (BRAIN Initiative Cell Census Network, 2021). This multi-institution collaboration is already producing innovative results (Muñoz-Castañeda et al., 2021) and actionable community resources (BICCN Data Ecosystem Collaboration, 2022).

Hippocampome.org is an open-access knowledge base of the rodent hippocampal circuit (dentate gyrus, CA3, CA2, CA1, subiculum, and entorhinal cortex) at the mesoscopic level of neuron types (Wheeler et al., 2015). This resource has proven popular and effective thanks to the adoption of a simple yet powerful classification system for defining neuron types. Specifically, a key property for the identification of neuron types in Hippocampome.org is the location of axons and dendrites across the subregions and layers of the hippocampal formation. This approach can be broadly extended to classify neurons in other brain regions and neural systems (Ascoli and Wheeler, 2016). Focusing on axonal and dendritic distributions provides several considerable advantages. First, these features mediate neuronal connectivity, thus immediately revealing the underlying blueprint of network circuitry (Rees et al., 2017). Second, they are widely used in the neuroscience community as a reliable and concrete anchoring signature to correlate electrophysiological and transcriptomic profiles (DeFelipe et al., 2013). Third, to coherently classify neuron types, we are not reliant on the inconsistent nomenclature that authors provide (Hamilton et al., 2017a). Therefore, starting from the foundational morphology-based identification of 122 neuron types in the first release (version 1.0 or v1.0), Hippocampome.org progressively amassed an increasing amount of complementary data, such as firing patterns (Komendantov et al., 2019), molecular expression (White et al., 2020), cell counts (Attili et al., 2022), synaptic communication (Moradi et al., 2022; Moradi and Ascoli, 2020), in vivo oscillations (Sanchez-Aguilera et al., 2021), and connection probabilities (Tecuatl et al., 2021b). In all cases, the public repository provided direct links to the specific peer-reviewed empirical evidence supporting the added knowledge.

Since the inception of Hippocampome.org, we have attempted to maintain the naming styling for already established neuron types by adopting either canonical names, only-cited names, most frequently cited names or hybridizations of cited names, and only as last resort crafting our own names (see Figure 6 in Hamilton et al., 2017a). In the entorhinal cortex (EC), where many of the hybridizations occur, we have followed the authors' own definitions for the six layers and the distinction between medial and lateral, when incorprating such terms into Hippocampome.org type names. If a neuron type exists in both medial and lateral entorhinal cortex, then the name is simply prefixed by EC, rather than MEC or LEC. As another example, in the dentate gyrus (DG), we established HIPROM (Hilar Interneuron with PRojections to the Outer Molecular layer) and MOCAP (MOlecular Commissural-Associational Pathway-related axons and dendrites) in the same vein as HIPP (HIlar Perforant Path-associated), MOPP (MOlecular layer Perforant Path-associated), and HICAP (HIlar Commissural-Associational Pathway-

related), where the outer two-thirds of the stratum moleculare (SMo) is distinguished by the region intercepted by the Perforant Path from the entorhinal cortex, and the inner one-third (SMi) is characterized by the commissural-associational pathway that often recurrently connects stratum moleculare with the hilus.

Having established a web-based integrated storehouse of hippocampal information, Hippocampome.org also expanded its scope by including data-driven computational models of neuronal excitability and synaptic signaling, as well as ties to community resources such as NeuroMorpho.Org (Akram et al., 2018), SenseLab ModelDB (McDougal et al., 2017), CARLsim (Niedermeier et al., 2022), and the Allen Brain Atlas (Jones et al., 2009). Altogether, these extensions resulted in the emergence of a complete framework in Hippocampome.org v2.0 that makes the original vision of this project, to enable data-driven spiking neural network simulations of rodent hippocampal circuits (Ascoli, 2010), finally achievable. The present report thus marks a new phase in the life cycle of this community resource.

One line of research pertaining to the state of simulation readiness of Hippocampome.org involves a real-scale mouse model of CA3 (Kopsick et al., 2022) investigating the cellular mechanisms of pattern completion, which includes Pyramidal cells and seven main inhibitory interneuron types. Another avenue of research investigates spatial representation involving *in vivo* firing grid cells (Sargolini et al., 2006), which utlizes Medial Entorhinal Cortex Layer II Stellate cells, two types of pyramidal cells, and three interneuron types. Both lines of research make use of Hippocampome.org parameters for properties such as cell census, Izhikevich models (Izhikevich, 2003), synaptic signals, and connection probabilities.

The following “Description of resource” section begins with a concise, referenced overview of the neural properties collated from Hippocampome.org v1.0 through release v1.12. We then briefly describe the new neuron types and data currently being added in Hippocampome.org v2.0. Next is an abridged summary of the usage and recognition of this online portal in biomedical research. This is followed by an explanation of the latest capabilities of Hippocampome.org v2.0 to search, filter, and download the complete set of computational parameters enabling quantitative connectomic analyses and spiking neural network simulations. The section concludes with an outlook of possible research applications allowed by the expansion of this scientific resource.

Description of resource

Characterizing properties of hippocampal neuron types

Hippocampome.org v1.0 (Wheeler et al., 2015) established the morphological encoding of axonal and dendritic locations and the main neurotransmitter (glutamate or GABA) as the primary determinants of neuron types in the rodent hippocampal formation. For example, a Dentate Gyrus Basket cell (with name capitalized to indicate a formally defined neuron type) is a GABAergic cell with axon contained in the granular layer and dendrites spanning all dentate gyrus layers (Figures 1A1-4). In this framework, two neurons releasing the same neurotransmitter belong to different types if the axon or dendrites of only one of them invades any of the 26 layers across 6 subregions of the hippocampal formation (hippocampome.org/morphology). In other words, neurons of the same type share the same potential inputs, outputs, and excitatory vs. inhibitory function. These properties were initially supplemented with additional empirical evidence for molecular expression of major protein biomarkers (Figure 1A5;

hippocampome.org/markers) and membrane biophysics (Figure 1A6-7; hippocampome.org/electrophysiology).

Many neuronal properties and functionalities were progressively added in 12 subsequent releases (Table 1). The numerical sequencing of these Hippocampome.org versions depended on the order of peer-review and publication of the corresponding scientific reports. Here we will describe them instead in logical groupings. The first two updates enhanced the user functionality of the knowledge base. Specifically, v1.1 integrated a web-based interactive thesaurus mapping of synonyms and definitions (Hamilton et al., 2017a; hippocampome.org/find-term) to help disambiguate the many terminological inconsistencies in the neuroscience literature (Shepherd et al., 2019; Yuste et al., 2020). Release v1.2 introduced the capability to browse, search, and analyze the potential connectivity between neuron types (Rees et al., 2016; Hippocampome.org/connectivity) as derived from the compiled overlapping locations of all the presynaptic axons and postsynaptic dendrites. Transcriptomic information was greatly expanded in both v1.3 (Hamilton et al., 2017b), which incorporated in situ hybridization data from the Allen Brain Atlas (Lein et al., 2007), and v1.5 (White et al., 2020), which leveraged relational inferences interlinking the region-specific expression of two or more genes.

The quantifications of firing pattern phenotypes, such as rapid adapting spiking, transient stuttering, and persistent slow-wave bursting, in v1.6 (Komendantov et al., 2019; hippocampome.org/firing_patterns) were fitted by dynamical systems modeling (Izhikevich, 2003) in v1.7 (Venkadesh et al., 2019; hippocampome.org/Izhikevich). Although the above properties were largely measured from slice preparations, v1.9 made available measurements from *in vivo* recordings (Sanchez-Aguilera et al., 2021; hippocampome.org/in-vivo). Release v1.10 provided a compendium of cognitive functions linked to specific hippocampal neurons (Sutton and Ascoli, 2021; hippocampome.org/cognome), while the v1.11 neuron type census estimated the population counts for each neuron type (Attili et al., 2022; hippocampome.org/census). Finally, are a set of properties pertaining not to individual neuron types but to synaptic connections between a pair of pre- and post-synaptic neuron types. In particular, v1.8 calculated the synaptic probabilities and the numbers of contacts per connected pair (Tecuatl et al., 2021b; hippocampome.org/syn_probabilities), and v1.4 data mined synaptic physiology (Moradi and Ascoli, 2020; hippocampome.org/synaptome), with conductance, time constant, and short-term plasticity values normalized by age, temperature, species, sex, and recording method in v1.12 (Moradi et al., 2022; hippocampome.org/synapse), leveraging machine learning and a phenomenological model (Tsodyks et al., 1998).

Expanding the catalog of neuron types and properties from Hippocampome.org v1.x to v2.0

The Hippocampome.org framework to classify neuron types and collate their properties allows agile content updates as new data are continuously reported in the peer-reviewed literature. For example, the description of a parvalbumin-positive dentate gyrus GABAergic interneuron with axon contained in the granular layer and dendrites invading the molecular layer but not the hilus (Vaden et al., 2020) supported the definition of a new neuron type (Figures 1B1-5), referred to in Hippocampome.org v2.0 as DG Basket GRALDEN (GRAnular Layer DENdrites) cell. Moreover, such an identification made it possible to unequivocally ascribe to this neuron type previously reported electrophysiological characteristics (Figures 1B6-7; Markwardt et al., 2011). Comprehensive literature mining following the same process expanded the Hippocampome.org v2.0 catalog with 56 new neuron types across 5 of the 6 subregions of the hippocampal formation (Figure 2), including axonal-dendritic morphological patterns (Figure 2A), molecular expression (Figure 2B), and membrane biophysics (Figure 2C).

Besides identifying new neuron types, the Hippocampome.org classification system also allows the ongoing accumulation of new properties onto existing neuron types as well as the reconciliation of fragmented descriptions from scientific publications (Figure 3). For instance, converging evidence indicates that Entorhinal Cortex Layer III Pyramidal cells have axonal projections in all layers of CA1 (Deller et al., 1996; Takács et al., 2012), not just in stratum lacunosum-moleculare (SLM) as originally reported (Steward, 1976). Hippocampome.org v2.0 captures both the new extracted knowledge and the corresponding experimental evidence (Figure 3A). The annotation of neuron type-specific firing phases relative to *in vivo* oscillations in v1.9 highlighted a clear distinction between Superficial and Deep CA1 Pyramidal cells (Sanchez-Aguilera et al., 2021). The present release enriches that description with accompanying novel molecular markers (Figure 3B1), membrane biophysics values (Figure 3B2), and differential connectivity with other subregions and neuron types (Figure 3B3). Similarly, numerous additional firing patterns (Figure 3C) have been datamined for existing neuron types, such as adapting spiking in CA1 Oriens-Bistratified cells (Craig and McBain, 2015), non-adapting spiking in CA3 Basket Cholecystokinin-positive (CCK+) cells (Szabadics and Soltesz, 2009) or transient stuttering in CA1 Radiatum Giant cells (Kirson and Yaari, 2000). Notably, this includes a novel phenotype, transient stuttering followed by persistent stuttering (TSTUT.PSTUT) in CA1 Interneuron Specific O-targeting QuadD cells (Chamberland et al., 2010). With this report, we also release new differential connection probabilities to various CA1 neuron type targets from traditional CA3 Pyramidal cells vs. CA3c Pyramidal cells (Figure 3D) and from Dentate Gyrus Granule cells to mossy fiber CA3 targets (Table 2).

Quantifying the content and impact of Hippocampome.org

Over the course of subsequent releases, we have measured Hippocampome.org content using two metrics. The number of pieces of knowledge (PoK) tallies the distinct units of structured information, such as the statements that Dentate Gyrus Granule cell axons invade the hilus or that CA1 Basket cells express parvalbumin. The pieces of evidence (PoE) are specific excerpts of peer reviewed publications (portion of text, figure, or table) or database entries (e.g., from the Allen Brain Atlas) always linked to each PoK. Both PoK and PoE continued to grow with successive releases of Hippocampome.org (Figure 4A). Notably, the largest increases in PoK and PoE were related to synaptic properties (Moradi and Ascoli, 2020; Tecuatl et al., 2021b; Moradi et al., 2022). Specifically, the data underlying synaptic physiology and connection probabilities were supported by over 23,000 PoE and yielded a remarkable 500,000 PoK thanks to the normalized collection of signaling and short-term plasticity modeling parameters for multiple combinations of experimental conditions.

To assess community usage of Hippocampome.org, we tracked the number of citations of the original publication (Wheeler et al., 2015) and of the subsequent versions (Figure 4B), separating simple references from actual employment of information extracted from Hippocampome.org for secondary analyses (Table 3). At the time of this writing, year 2021 proved to be the most prolific citation-wise; however, more than a third of the releases (v1.8-12) appeared after 2021 and most PoK were added in 2022, so usage could potentially accelerate further in coming years. An early application of Hippocampome.org-sourced data used subthreshold biophysical measures, such as input resistance and membrane time constant, for multicompartmental models of signal integration and extracellular field generation (Gulyas et al., 2016). That study concluded that somatic and proximal dendritic intracellular recordings in pyramidal cells and calretinin-positive interneurons, in particular, do not capture a sizable portion of the synaptic inputs. As a recent usage example, another lab employed Hippocampome.org as the primary information resource for neuron types in DG, CA3, and CA1 (Schumm et al., 2022). They discovered that mild traumatic brain injury, in the form of alterations in spike-timing-dependent

plasticity, may affect the broadband power in CA3 and CA1 and the phase coherence between CA3 and CA1.

From experimental data to biologically realistic computational models

Several key neural properties collated into Hippocampome.org have gradually transformed the site from an organized repository of hippocampal knowledge to a computational framework for launching real-scale neural network simulations. Specifically, building a data-driven circuit model of a neural system (such as the hippocampal formation or portion thereof) requires four essential quantities besides the full list of neuron types (Bahmer et al., 2023; DePasquale et al., 2023): (i) the number of neurons in each type; (ii) the input-output response function for each neuron type; (iii) the connection probability for each pair of interacting neuron types; and (iv) the unitary synaptic signals for each pair of connected neuron types (Figure 5). Of those quantities, (i) and (ii) are neuron type properties, while (iii) and (iv) are properties of directional connections, defined as a distinct pair of a presynaptic and a postsynaptic neuron type. Moreover, (i) and (iii) are structural features, while (ii) and (iv) are electrophysiological ones.

Hippocampome.org v1.11 provides estimates of the number of neurons in each neuron type (i) for both rats and mice (Figure 5A). These values were derived in a two-step process (Attili et al., 2020): first, literature mining extracted suitable quantitative relations such as the cellular density in a given layer (Attili et al., 2019), the total count of neurons expressing a certain gene, or the fraction of sampled cells with a particular morphology; second, numerical optimization of the corresponding equations yielded a complete census for all neuron types. As of v1.7, Hippocampome.org represents the neuronal input-output response function (ii) in the form of single- and multi-compartment Izhikevich models (Figure 5B) fitted by evolutionary algorithms to accurately reproduce the observed firing behavior of each neuron type (Venkadesh et al., 2018). For v1.8, the connection probability (iii) from one neuron type to another (Figure 5C) was computed from measurements of the appropriate axonal and dendritic lengths in each invaded subregion and layer (hippocampome.org/A-D_lengths). Additionally, users can also access the presynaptic and postsynaptic path distances from the respective somata (hippocampome.org/soma_distances) and the number of contacts per connected neuron pairs (hippocampome.org/num_contacts). As for the synaptic communication between neurons (iv), Hippocampome.org v1.12 adopted the Tsodyks-Pawelzik-Markram formulation, representing unitary signals and short-term plasticity with five constants for each directional pair of interacting neuron types: the synaptic conductance, decay time, recovery time, facilitation time, and the utilization ratio (Tsodyks et al., 1998; Moradi et al., 2022). Once again, these parameters were fitted from the experimental data (Moradi and Ascoli, 2018) employing deep learning to account for (and predict the effects of) numerous experimental variables (Figure 5D), including species (rat vs. mouse), sex (male vs. female), age (young vs. adult), recording temperature (room vs. body), and clamping configuration (voltage vs. current).

The above description underscores the crucial interconnectedness of individually measured neuronal properties forming a cohesive whole in Hippocampome.org (Figure 6). In particular, normalized simulation parameters (e.g., the sensitivity of recovery variable in Izhikevich models) are derived from quantitative experimental measurements, such as the spiking adaptation rate (Figure 6a). Those in turn are linked to an identified neuron type based on qualitative features, like calbindin expression or laminar distribution of axons and dendrites. In addition to enabling computational applications as described below, such integration also allows the meta-analysis of correlations between morphological features, molecular profiles, electrophysiological properties, and dynamic circuit functions. At the same time, several components of Hippocampome.org are also synergistically linked to external community

resources (Figure 6B). For example, each neuron page links out to all three-dimensional morphological reconstructions of the same cell type available in NeuroMorpho.Org (Ascoli et al., 2007), and selected data from NeuroMorpho.Org were used to compute axonal and dendritic length and connection probabilities. Each neuron page also links out to all computational models (including Hodgkin-Huxley, stochastic diffusion, mean firing rate, etc.) involving the same cell type on ModelDB (McDougal et al., 2017), while conversely ModelDB includes the Izhikevich models for all Hippocampome.org neuron types. Moreover, simulation parameters from Hippocampome.org are exportable to the CARLsim simulation environment (Nageswaran et al., 2009), enabling fast execution of spiking neural network models optimized for GPUs. Furthermore, Hippocampome.org harnessed data from the Allen Brain Atlas (Lein et al., 2007) to infer gene expression for principal neurons and cell densities for use in the neuron type census.

To facilitate construction of spiking neural network simulations, Hippocampome.org v2.0 also includes a new graphical user interface (GUI). With this GUI, users can download sets of simulation parameter values for arbitrarily selected neuron types, a subregion of interest, or the whole hippocampal formation (Figure 7). The sets consist of files for the instantiation of CARLsim simulations and a comma-separated values (CSV) spreadsheet of parameters for use in a different simulation environment of the user's choice. For the convenience of users interested in simplified circuit models, Hippocampome.org informally ranks the importance of each neuron type in terms of the functional role it plays in the hippocampal circuitry from 1 (essential) to 5 (dispensable). For instance, a user may choose to simulate only the canonical, or rank 1, neuron types of the tri-synaptic circuit and entorhinal cortex, consisting of Dentate Gyrus Granule, CA3 Pyramidal, CA1 Pyramidal, and Medial Entorhinal Cortex Layer II Stellate cells. When Hippocampome.org is missing a parameter value due to insufficient experimental evidence, the GUI exports a default value clearly indicating so in the downloadable files. For missing Izhikevich and synaptic signaling parameters, the default values are those provided by the CARLsim simulation environment. For missing synaptic probabilities, Hippocampome.org precomputes values averaged by connection type, namely excitatory-excitatory (0.0117), excitatory-inhibitory (0.0237), inhibitory-excitatory (0.00684), and inhibitory-inhibitory (0.00423).

Potential applications to connectomic analyses and spiking neural networks simulations

Hippocampome.org v2.0 enables the multiscale analysis of circuit connectivity (Figure 8). At the highest echelon are the connections between hippocampal subregions, which are comprised of the mesoscopic level potential connectivity between individual neuron types (Figure 8A). Expanding, for example, upon the 147 connections between the dentate gyrus and CA3 neuron types reveals all the connections every individual neuron type forms with the other neuron types within and across the subregions (Figure 8B). Zooming in onto a single neuron type each from the dentate gyrus and CA3, it is possible to quantify the efferent and afferent connections with other neuron types from throughout the hippocampal formation in terms of synaptic probabilities and number of neuronal partners (Figure 8C). Diving even deeper into the isolated connection between two neuron types, such as the mossy fiber contacts from Dentate Gyrus Granule cells to CA3 Basket cells, expands the connectivity analysis to several physiological factors affecting neuronal communication: the subcellular location of the synaptic contact (e.g., soma in *stratum pyramidale* and proximal dendrites in *stratum lucidum*), the transfer function (product of synaptic conductance and decay time constant), the *in vivo* firing rate of the presynaptic neuron type, and the relationship between input current and resulting output spiking frequency (F-I curve) of the post-synaptic neuron (Figure 8D).

Release of v2.0 makes the original objective of Hippocampome.org, to enable data-driven spiking neural network simulations of rodent hippocampal circuits (Ascoli, 2010), finally achievable. An ongoing line of research in this regard focuses on a real-scale mouse model of CA3, with the eventual goal of investigating the cellular mechanisms of pattern completion. Initial work included excitatory Pyramidal cells and seven main inhibitory interneuron types: Axo-axonic cells (AAC), Basket cells (BC), Basket Cholecystokinin-positive cells (BC CCK+), Bistratified cells (BiC), Ivy cells, Mossy Fiber-Associated ORDEN (MFA ORDEN) cells, and QuadD-LM (QuadD) cells (Kopsick et al., 2022). Use of Hippocampome.org parameters for cell census, Izhikevich models, synaptic signals, and connection probabilities resulted in robust, realistic, rhythmic resting state activity for all neuron types (Figure 9A). Building off the constructed network of CA3, we seek to understand how the neuron type circuit may allow for the formation of cell assemblies that correspond to distinct memories. Additionally, we will evaluate the network's pattern completion capabilities when presented with degraded input patterns (Guzman et al., 2021). Furthermore, associations between memories in CA3 may be encoded by cells shared between cell assemblies (Gastaldi et al., 2021). Therefore, we will investigate how cell assembly size and overlap may impact memory storage and recall and the role of different neuron types in associating cell assemblies with one another.

Another pursuit using a spiking neural network seeks to replicate the spatial representation in grid cells (Sargolini et al., 2006), modeled utilizing Hippocampome.org Medial Entorhinal Cortex Layer II Stellate cells (SC), and supported by various GABAergic interneuron types (Dhillon and Jones, 2000): Axo-axonic (AA), Basket cells (BC), and Entorhinal Cortex Layer II Basket-Multipolar cells (BC MP). This study aims to reproduce the *in vivo* firing of these neuron types as a virtual rodent explores an open field (Figure 9B). Different theories offer potential neural mechanisms underlying the grid cell phenomenon, but it remains challenging to test them comprehensively for anatomical and electrophysiological consistency with experimental data (Sutton and Ascoli, 2021; Zilli, 2012). Our current work demonstrates that a spiking neural network implementation of one such theory, the continuous attractor model, generates grid field activity highly compatible with that measured in behaving animals when utilizing Hippocampome.org model parameters. While preliminary, these illustrative examples highlight the potential of Hippocampome.org-enabled data-driven spiking neural network simulations to investigate computational theories of cognitive functions in hippocampal circuits at the level of biologically detailed mechanisms.

Discussion

Hippocampome.org, through its continuous updates and conspicuous usage, has established itself prominently amongst other readily accessible, evidence-based, expert-curated bioscience public resources of note, such as FlyBase for *Drosophila* molecular biology (The FlyBase Consortium, 1994; dos Santos et al., 2015), WormBase for nematode genomics (Stein et al., 2001), the Blue Brain Project for somatosensory cortex (Markram, 2006), SynGO for synaptic functions (Koopmans et al., 2019), and RegenBase for spinal cord injury biology (Callahan et al., 2016). Hippocampome.org has evolved from being a storehouse of information in v1.0-1.12, along the lines of FlyBase, WormBase, SynGO, and RegenBase, to a platform in v2.0 for launching detailed simulations of the hippocampal formation, in the vein of the Blue Brain Project. However, Hippocampome.org distinguishes itself in its reliance wholly on already published data and the more tailored focus on a single portion of the brain.

The foundation for Hippocampome.org has always been the data that are published in the literature. Although a certain level of interpretation is always necessary to make the data machine readable and

suitable for database incorporation, data inclusion does not depend on how the data are modeled. Nevertheless, some of the simulation-ready parameters now also included in Hippocampome.org are indeed the result of modeling, such as the neuronal input/output functions (Izhikevich model; Izhikevich, 2003) and the unitary synaptic values (Tsodyks-Pawelzik-Markram model; Tsodyks et al., 1998). Other simulation-ready parameters are the result of specific analysis approaches, including the connection probabilities (axonal-dendritic spatial overlaps) and the neuron type census (numerical optimization of all constraints).

The growth of Hippocampome.org since the initial release of v1.0 (Wheeler et al., 2015) has been prodigious. To date, the site has been visited over 136,000 times with over 33,000 unique visits, and the original publication has been cited more than hundred times. Each successive release of Hippocampome.org v1.X has added new dimensions of knowledge and/or functionality and has been building toward assembling all the components necessary to produce real-scale computational models of the rodent hippocampal formation. The culmination of all this work is the release of Hippocampome.org v2.0, which introduces a framework for launching computer simulations directly from the accumulated knowledge. However, achieving simulations does not mark the end point for this project, because Hippocampome.org will continue to aggregate new knowledge as it is published in the peer-reviewed literature. Gradually, the focus of this resource will shift from development to exploitation through the in silico emulation of complex dynamics observed *in vivo* and *in vitro*, with the goal of shedding light on the underlying synaptic-level computational mechanisms.

The creation of real-scale spiking neural network models of the hippocampal formation and its subregions can foster biologically realistic, data-driven, mesoscopic simulations of cognitive function and dysfunction (Sutton and Ascoli, 2021). For instance, simulations with Hippocampome.org's real-scale model of the dentate gyrus can build on previous network models of epileptogenesis (Dyhrfjeld-Johnsen et al., 2007) by providing further clarity to the roles of all documented neuron types and their corresponding potential connections in seizure initiation and propagation. A real-scale model of CA1 can aim to further the insights into the spatiotemporal dynamics of the circuit during theta oscillations (Bezaire et al., 2016; Navas-Olive et al., 2020; Romani et al., 2023). Furthermore, network models involving multiple subregions can open new vistas on unexplored territories, such as the use of real-scale models of the entorhinal cortex and CA2 to simulate the neuron- and connection-type specific mechanisms of social memory (Lopez-Rojas et al., 2022). Moreover, open source sharing of the real-scale models replicating those functions (Gleeson et al., 2017) will facilitate cross-talk within the systems neuroscience community to better understand the role of distinct neuron types in hippocampal function.

A notable aspect of Hippocampome.org is that all freely downloadable model parameters are directly linked to the specific peer-reviewed empirical evidence from which they were derived. Thus, if users disagree with a specific interpretation, or are not fully convinced by an individual experimental measurement, they maintain control in selecting the information sources. Conversely, researchers can choose to reuse the collated experimental data to constrain different computational models they may prefer, such as adopting the Hodgkin-Huxley formalism instead of Izhikevich dynamics. At the same time, Hippocampome.org is not only a collection of model parameters and corresponding empirical evidence, but it also provides an opportunity to unearth knowledge gaps, as facilitated by an intuitive search functionality (hippocampome.org/find-neuron). Missing data can serve to guide the design of targeted "low hanging fruit" experiments or to generate new hypotheses.

Another important element of Hippocampome.org is the careful annotation of the experimental metadata for each piece of evidence, including the species (rat or mouse), sex (male or female), age (young or adult) as well as any and all reported details that could affect the recorded neuronal property. Examples of these confounding factors abound especially for *in vitro* electrophysiological data, such as the exact chemical composition of the solution in the electrode and in the bath, slice thickness and orientation, clamping configuration, recording temperature, and animal weight. Because these covariates, when reported by the original investigators, are also stored in the database, it is possible to account for them in subsequent analyses and simulations. Hippocampome.org therefore constitutes a considerably rich one-stop resource to compare and "translate" key parameters, such as the amplitude and duration of a synaptic signal between two specifically identified neuron types, for instance, from 14 day old male rat at 22 ˚C in voltage clamp to a 56 day old female mouse at 32 ˚C in current clamp. When fed into spiking neural network simulations, these differential parameter values can foster intuition while attempting to reconcile neuroscience theories and observations.

Hippocampome.org is yet poised for the onset of an information deluge from current and future big science projects, which will need to be integrated into a complete cohesive picture (de La Prida and Ascoli, 2021). Although morphological identification will continue to play a fundamental role in defining neuron types and circuit connectivity, the manner in which knowledge is cross-referenced in this resource will allow its effective linkage to rapidly accumulating molecular and imaging data. The ongoing spatial transcriptomics revolution is already transforming the frontiers of cellular neuroscience, often using the hippocampus as its favorite sandbox (Lein et al., 2017; Yao et al., 2021; Zeisel et al., 2015). Single-cell transcriptomics via scRNAseq can bolster the current morphological information by offering distinct transcription factor codes for existing neuron types and assist in defining new ones (Cembrowski and Spruston, 2019; Winnubst et al., 2020; Yuste et al., 2020). From the functional side, optical imaging via genetically encoded voltage indicators (Knöpfel and Song, 2019) will provide *in vivo* voltage traces for defined neuron types that can greatly enhance the repertoire of firing pattern phenotypes to utilize in simulations (Adam et al., 2019). Data-driven computational models can provide a useful conceptual bridge between molecular sequencing and activity imaging by investigating the effects of specific subcellular distributions of voltage- and ligand-gated conductances on neuronal excitability (Migliore et al., 2018). With the converging maturation of these young techniques and the advent of others yet on the horizon, Hippocampome.org will be able to integrate multidimensional knowledge on the solid foundation of neuronal classification.

Materials and Methods

Hippocampome.org v2.0 vs. the legacy status of v1.12

With the release of v2.0 of Hippocampome.org upon publication of this article, v1.12 of the website will no longer be updated and will transition to legacy status (hippocampome.org/legacy_v1). In this way, users may avail themselves of the full benefits of the new content and functionality of v2.0, while maintaining access to reference content as published through v1.12. In the near term, neuron types new to v2.0 are tagged with an asterisk on the web site to differentiate them from v1.X types.

Linking neuron types to NeuroMorpho.Org morphological reconstructions

Hippocampome.org neuron types are regularly linked to appropriately identified digital reconstructions of neuronal morphology from NeuroMorpho.Org (Ascoli et al., 2007). Identification of suitable

reconstructions with individual neuron types depends on the correspondence of dendritic and axonal locations across hippocampal subregions and layers, as they appear in the reference publication. Alternatively, direct cell typing by the authors in the reference publication text is accepted as evidence for canonical (principal cell) types, such as CA1 Pyramidal cells or Dentate Gyrus Granule cells. Reconstructions are not linked to a neuron type if the experimental conditions are inconsistent with the inclusion criteria of Hippocampome.org, as in the case of cell cultures or embryonic development. Lack of either axonal or dendritic tracing also disqualifies reconstructions of non-canonical neurons from being linked.

Connections from DG Granule cells to CA3

To compute estimates of connection probabilities and numbers of contacts per connected pair for the rat mossy fiber-CA3 circuit, we used previously calculated average convex hull volume (Tecuatl et al., 2021b) and several measurements from a seminal anatomical study (Acsády et al., 1998): DG Granule cell axonal length within CA3 (3,236 µm), inter-bouton distances for mossy boutons on Pyramidal cell targets in CA3c (162 µm) and in the rest of CA3 (284 µm), and inter-bouton distances for en-passant and filipodia boutons onto CA3 interneurons (67.4 µm, considering that 48 interneurons can be contacted by a single GC). Given that the mossy fibers innervate mainly CA3 SL, and due to the lack of information regarding the exact proportion of axons innervating CA3 SP, these calculations assume that GCs only innervate SL. The probabilities of connection and numbers of contacts per connected pair (Table 2) are estimated as previously described (Tecuatl et al., 2021a) utilizing the CA3 dendritic lengths reported in Hippocampome.org.

Connections from CA3 and CA3c Pyramidal cells to CA1

To compute estimates of connection probabilities and numbers of contacts per connected pair for the rat Schaffer collaterals-CA1 circuit, we utilized previously reported values for the distinct axonal innervation patterns (Ropireddy et al., 2011; Sik et al., 1993; Wittner et al., 2007) in CA1 *stratum radiatum* (SR) and *stratum oriens* (SO) from CA3 Pyramidal cells (27.5% of total axonal length: 64% to SR, 15% to *stratum pyramidale* (SP), 21% to SO) and CA3c Pyramidal cells (64.1% of total axonal length: 94% to SR, 3% to SP, 3% to SO). In addition, we used the average inter-bouton distance reported for the Schaffer collaterals (Li et al., 1994) in SR (4.47 µm) and SO (5.8 µm). Total axonal length was measured with L-Measure (Scorcioni et al., 2008) from three NeuroMorpho.Org reconstructions for CA3c (NMO_00187, NMO_00191) and CA3b (NMO_00931). We extracted parcel-specific convex hull volumes from Janelia MouseLight (Winnubst et al., 2019) Pyramidal cell reconstructions (AA0304, AA0307, AA0420, AA0960, AA0997, AA0999, AA1548) mapped to the 2022 version of the Allen Institute Common Coordinate Framework (CCF). The probabilities of connection and number of contacts per connected pair were estimated as previously described (Tecuatl et al., 2021a) using CA1 dendritic lengths from Hippocampome.org. We used separate values for inter-bouton distances in CA1 SR for CA3c Pyramidal cells (5.5 µm: Wittner et al., 2007) and CA3 Pyramidal cells (3.7 µm: Shepherd et al., 2002; 4.4 µm: Li et al., 1994; 4.29 µm: Sik et al., 1993; averaged as 4.1 µm).

Constructing Hippocampome.org spiking neural simulations

Hippocampome.org utilizes CARLsim (Nageswaran et al., 2009) as its default simulation environment (socsci.uci.edu/~jkrichma/CARLsim/). CARLsim is a graphics processing unit (GPU)-accelerated library of functions for simulating spiking neural networks based on Izhikevich neuron models (Izhikevich, 2003). We selected CARLsim due to this ability to run on collections of GPUs, , as the power of a GPU

supercomputer is needed to simulate the millions of neurons that comprise a full-scale spiking neural network simulation of the complete hippocampal formation. The current version is CARLsim 6 (Niedermeier et al., 2022), and the most up-to-date Hippocampome.org-optimized code base, including features not yet released in the main CARLsim version, can be found at hippocampome.org/CARLsim (Kopsick et al., 2022).

Web portal, database, and source code

Hippocampome.org runs on current versions of Chrome, Safari, and Edge web browsers, and it is deployed on a CentOS server running Apache. The website runs off of PHP from a MySQL database. The code for Hippocampome.org is available open source at github.com/Hippocampome-Org. This includes all code for displaying the pages of the website, all scripts for importing spreadsheets into the database, code for using evolutionary algorithms to optimize Izhikevich model parameters, code for the graph theory analysis of the potential connectome, code for the implementation of the firing pattern classification algorithm, and code for analyzing network simulations in CARLsim.

Glossary of abbreviations

5HT-3:	serotonin receptor 3
AA:	EC LII Axo-axonic cell
AAC:	Axo-axonic cell
ABA:	Allen Brain Atlas
AP_{ampl}:	action potential amplitude
AP_{width}:	action potential width
ASP.:	adapting spiking
Astn2:	astrotactin 2
BC:	Basket cell
BC MP:	EC LII Basket-Multipolar cell
BiC:	Bistratified cell
BICCN:	BRAIN Initiative Cell Census Network
C:	Capacitance
CB:	calbindin
CB1:	cannabinoid receptor type 1
CCK+:	cholecystokinin-positive
CR:	calretinin
CSV:	comma-separated value
Dcn:	decorin
DG:	dentate gyrus
E-E:	excitatory to excitatory
E-I:	excitatory to inhibitory
EC:	entorhinal cortex
ENK:	enkephalin
fAHP:	fast after-hyperpolarizing potential
g:	conductance constant
GABAa α1:	GABA-a alpha 1 subunit
GC:	granule cell
Gpc3:	glypican 3
GPUs:	graphical processing units

557 GRALDEN: GRAnule-Like DENdrites
558 Garci: grid cell
559 Grp: gastrin releasing peptide
560 GUI: graphical user interface
561 H: hilus
562 HIPROM: Hilar Interneuron with PRojections to the Outer Molecular layer
563 Htr2c: 5-hydroxytryptamine receptor 2c
564 I-E: inhibitory to excitatory
565 I-I: inhibitory to inhibitory
566 IS: interneuron specific
567 LI-II: layers 1-2
568 LII: layer 2
569 LIII: layer 3
570 Max FR: maximum firing rate
571 MEC: medial entorhinal cortex
572 MFA: Mossy Fiber-Associated
573 mGluR1a: metabotropic glutamate receptor 1 alpha
574 MOCAP: cell with MOlecular Commissural-Associational Pathway-related axons and dendrites
575 MOLAX: MOlecular Layer Axons
576 MP PC: EC LI-II Multipolar Pyramidal cell
577 Mus2R: muscarinic type 2 receptor
578 NASP: non-adapting spiking
579 Ndst4: N-deacetylase and N-sulfotransferase 4
580 nNOS: neuronal nitric oxide synthase
581 Nov: nephroblastoma overexpressed
582 NPY: neuropeptide Y
583 Nr3c2: nuclear receptor subfamily 3 group C member 2
584 Nr4a1: nuclear receptor subfamily 4 group A member 1
585 ORAX; ORiens AXons
586 ORDEN: ORiens DENdrites
587 PC: pyramidal cell / CA1 Pyramidal cell (Fig. 9B)
588 PL: polymorphic layer
589 PoE: pieces of evidence
590 PoK: pieces of knowledge
591 Prss12: serine protease 12
592 Prss23: serine protease 23
593 PV+: parvalbumin-positive
594 QuadD-LM: quadrilaminar dendrites – lacunosum-moleculare
595 R_{in}: input resistance
596 RLN: reelin
597 sAHP: slow after-hyperpolarizing potential
598 SC: MEC LII Stellate cell
599 SD: standard deviation
600 SG: stratum granulosum
601 SL: stratum lucidum
602 SLM: stratum lacunosum-moleculare
603 SMi: inner stratum moleculare
604 SMo: outer stratum moleculare

SO:	stratum oriens
SOM:	somatostatin
SP:	stratum pyramidale
SR:	stratum radiatum
Sub:	subiculum
SWR:	sharp-wave ripple
SynGO:	synaptic gene ontologies
T:	Temperature
τ_d:	synaptic decay constant
τ_f:	facilitation time constant
τ_m:	membrane time constant
τ_r:	recovery time constant
TPM:	Tsodyks-Pawelzik-Markram
TSTUT.:	transient stuttering
TSTUT.PSTUT:	transient stuttering followed by persistent stuttering
TSTUT.SLN:	silence preceded by transient stuttering
U:	utilization ratio
vGluT3:	vesicular glutamate transporter 3
V_h:	holding potential
VIP:	vasoactive intestinal polypeptide
V_{min}:	post-spike reset potential
V_{peak}:	spike cutoff potential
V_r / V_{rest}:	resting membrane potential
V_t / V_{thresh}:	firing threshold potential
WA BC:	Wide-arbor Basket cell
Wfs1:	wolframin ER transmembrane glycoprotein

Acknowledgements

We thank David J. Hamilton, Charise M. White, Christopher L. Rees, Maurizio Bergamino, Keivan Moradi, Siva Venkadesh, Alberto Sanchez-Aguilera, Teresa Jurado-Parras, Manuel Valero, Miriam S. Nokia, Elena Cid, Ivan Fernandez-Lamo, Daniel García-Rincón, Liset M. de la Prida, Sarojini M. Attili, Iqbal Addou, and the many student interns (hippocampome.org/thx) for invaluable help advancing from v1.0 to v2.0.

Competing Interests

The authors have no competing interests.

Contributions

DWW contributed to the conceptualization, methodology, software, investigation, data curation, writing – original draft, visualization, supervision, and project administration. JDK contributed to the methodology, software, formal analysis, investigation, data curation, writing – review and editing, and visualization. NS contributed to the methodology, software, investigation, data curation, writing – review and editing, and visualization. CT contributed to the methodology, validation, formal analysis, investigation, data curation, writing – review and editing, visualization, and supervision. AOK contributed to the formal analysis, writing – review and editing, and visualization. KN contributed to the software and writing – review and editing. GAA contributed to the conceptualization, methodology,

resources, investigation, data curation, writing – review and editing, visualization, supervision, project administration, and funding acquisition.

Funding information

This work was supported in part by grants R01NS39600, RF1MH128693, and U01MH114829 from the National Institutes of Health (NIH), and DE-SC0022998 from the Department of Energy (DOE). The funding sources were not involved in study design, data collection and interpretation, or the decision to submit the work for publication.

References

Acsády L, Kamondi A, Sík A, Freund T, Buzsáki G. 1998. GABAergic cells are the major postsynaptic targets of mossy fibers in the rat hippocampus. *The Journal of Neuroscience: The Official Journal of the Society for Neuroscience* **18**:3386–3403. doi:10.1523/JNEUROSCI.18-09-03386.1998

Adam Y, Kim JJ, Lou S, Zhao Y, Xie ME, Brinks D, Wu H, Mostajo-Radji MA, Kheifets S, Parot V, Chettih S, Williams KJ, Gmeiner B, Farhi SL, Madisen L, Buchanan EK, Kinsella I, Zhou D, Paninski L, Harvey CD, Zeng H, Arlotta P, Campbell RE, Cohen AE. 2019. Voltage imaging and optogenetics reveal behaviour-dependent changes in hippocampal dynamics. *Nature* **569**:413–417. doi:10.1038/s41586-019-1166-7

Aery Jones EA, Rao A, Zilberter M, Djukic B, Bant JS, Gillespie AK, Koutsodendris N, Nelson M, Yoon SY, Huang K, Yuan H, Gill TM, Huang Y, Frank LM. 2021. Dentate gyrus and CA3 GABAergic interneurons bidirectionally modulate signatures of internal and external drive to CA1. *Cell Reports* **37**:110159. doi:10.1016/j.celrep.2021.110159

Akram MA, Nanda S, Maraver P, Armañanzas R, Ascoli GA. 2018. An open repository for single-cell reconstructions of the brain forest. *Scientific Data* **5**:180006. doi:10.1038/sdata.2018.6

Amunts K, Ebell C, Muller J, Telefont M, Knoll A, Lippert T. 2016. The Human Brain Project: Creating a European Research Infrastructure to Decode the Human Brain. *Neuron* **92**:574–581. doi:10.1016/j.neuron.2016.10.046

Ascoli GA, Donohue DE, Halavi M. 2007. NeuroMorpho.Org: a central resource for neuronal morphologies. *The Journal of Neuroscience: The Official Journal of the Society for Neuroscience* **27**:9247–9251. doi:10.1523/JNEUROSCI.2055-07.2007

Ascoli GA, Wheeler DW. 2016. In search of a periodic table of the neurons: Axonal-dendritic circuitry as the organizing principle: Patterns of axons and dendrites within distinct anatomical parcels provide the blueprint for circuit-based neuronal classification. *BioEssays* **38**:969–976. doi:10.1002/bies.201600067

Attili SM, Mackesey ST, Ascoli GA. 2020. Operations research methods for estimating the population size of neuron types. *Annals of Operations Research* **289**:33–50. doi:10.1007/s10479-020-03542-7

Attili SM, Moradi K, Wheeler DW, Ascoli GA. 2022. Quantification of neuron types in the rodent hippocampal formation by data mining and numerical optimization. *The European Journal of Neuroscience* **55**:1724–1741. doi:10.1111/ejn.15639

Attili SM, Silva MFM, Nguyen T, Ascoli GA. 2019. Cell numbers, distribution, shape, and regional variation throughout the murine hippocampal formation from the adult brain Allen Reference Atlas. *Brain Structure and Function* **224**:2883–2897. doi:10.1007/s00429-019-01940-7

Bahmer A, Gupta D, Effenberger F. 2023. Modern Artificial Neural Networks: Is Evolution Cleverer? *Neural Computation* **35**:763–806. doi:10.1162/neco_a_01575

Bezaire MJ, Raikov I, Burk K, Vyas D, Soltesz I. 2016. Interneuronal mechanisms of hippocampal theta oscillations in a full-scale model of the rodent CA1 circuit. *eLife* **5**:e18566. doi:10.7554/eLife.18566

706 BICCN Data Ecosystem Collaboration, Hawrylycz MJ, Martone ME, Hof PR, Lein ES, Regev A,
707 Ascoli GAA, Bjaalie JG, Dong H-W, Ghosh SS, Gillis J, Hertzano R, Haynor DR, Kim Y, Liu Y,
708 Miller JA, Mitra PP, Mukamel E, Osumi-Sutherland D, Peng H, Ray PL, Sanchez R,
709 Ropelewski A, Scheuermann RH, Tan SZK, Tickle T, Tilgner H, Varghese M, Wester B,
710 White O, Aevermann B, Allemang D, Ament S, Athey TL, Baker PM, Baker C, Baker KS,
711 Bandrowski A, Bishwakarma P, Carr A, Chen M, Choudhury R, Cool J, Creasy H, D'Orazi F,
712 Degatano K, Dichter B, Ding S-L, Dolbeare T, Ecker JR, Fang R, Fillion-Robin J-C, Fliss TP,
713 Gee J, Gillespie T, Gouwens N, Halchenko YO, Harris N, Herb BR, Hintiryan H, Hood G,
714 Horvath S, Jarecka D, Jiang S, Khajouei F, Kiernan EA, Kir H, Kruse L, Lee C, Lelieveldt B, Li
715 Y, Liu H, Markuhar A, Mathews J, Mathews KL, Miller MI, Mollenkopf T, Mufti S, Mungall
716 CJ, Ng L, Orvis J, Puchades MA, Qu L, Receveur JP, Ren B, Sjoquist N, Staats B, Thompson
717 CL, Tward D, Van Velthoven CTJ, Wang Q, Xie F, Xu H, Yao Z, Yun Z, Zeng H, Zhang G-Q,
718 Zhang YR, Zheng JW, Zingg B. 2022. The BRAIN Initiative Cell Census Network Data
719 Ecosystem: A User's Guide (preprint). Bioinformatics. doi:10.1101/2022.10.26.513573
720 Callahan A, Abeyruwan SW, Al-Ali H, Sakurai K, Ferguson AR, Popovich PG, Shah NH, Visser U,
721 Bixby JL, Lemmon VP. 2016. RegenBase: a knowledge base of spinal cord injury biology
722 for translational research. *Database: The Journal of Biological Databases and Curation*
723 **2016**:baw040. doi:10.1093/database/baw040
724 Cembrowski MS, Spruston N. 2019. Heterogeneity within classical cell types is the rule: lessons
725 from hippocampal pyramidal neurons. *Nature Reviews Neuroscience* **20**:193–204.
726 doi:10.1038/s41583-019-0125-5
727 Chamberland S, Salesse C, Topolnik D, Topolnik L. 2010. Synapse-specific inhibitory control of
728 hippocampal feedback inhibitory circuit. *Frontiers in Cellular Neuroscience* **4**:130.
729 doi:10.3389/fncel.2010.00130
730 Ciarpella F, Zamfir RG, Campanelli A, Ren E, Pedrotti G, Bottani E, Borioli A, Caron D, Di Chio M,
731 Dolci S, Ahtiainen A, Malpeli G, Malerba G, Bardoni R, Fumagalli G, Hyttinen J, Bifari F,
732 Palazzolo G, Panuccio G, Curia G, Decimo I. 2021. Murine cerebral organoids develop
733 network of functional neurons and hippocampal brain region identity. *iScience*
734 **24**:103438. doi:10.1016/j.isci.2021.103438
735 Craig MT, McBain CJ. 2015. Fast gamma oscillations are generated intrinsically in CA1 without
736 the involvement of fast-spiking basket cells. *The Journal of Neuroscience: The Official*
737 *Journal of the Society for Neuroscience* **35**:3616–3624. doi:10.1523/JNEUROSCI.4166-
738 14.2015
739 de La Prida LM, Ascoli GA. 2021. Explorers of the cells: Toward cross-platform knowledge
740 integration to evaluate neuronal function. *Neuron* **109**:3535–3537.
741 doi:10.1016/j.neuron.2021.10.025
742 DeFelipe J, López-Cruz PL, Benavides-Piccione R, Bielza C, Larrañaga P, Anderson S, Burkhalter
743 A, Cauli B, Fairén A, Feldmeyer D, Fishell G, Fitzpatrick D, Freund TF, González-Burgos G,
744 Hestrin S, Hill S, Hof PR, Huang J, Jones EG, Kawaguchi Y, Kisvárday Z, Kubota Y, Lewis
745 DA, Marín O, Markram H, McBain CJ, Meyer HS, Monyer H, Nelson SB, Rockland K,
746 Rossier J, Rubenstein JLR, Rudy B, Scanziani M, Shepherd GM, Sherwood CC, Staiger JF,
747 Tamás G, Thomson A, Wang Y, Yuste R, Ascoli GA. 2013. New insights into the
748 classification and nomenclature of cortical GABAergic interneurons. *Nature Reviews*
749 *Neuroscience* **14**:202–216. doi:10.1038/nrn3444

750 Deller T, Adelmann G, Nitsch R, Frotscher M. 1996. The alvear pathway of the rat hippocampus.
751 *Cell and Tissue Research* **286**:293–303. doi:10.1007/s004410050699
752 Depannemaecker D, Canton Santos LE, Rodrigues AM, Scorza CA, Scorza FA, Almeida A-CG de.
753 2020. Realistic spiking neural network: Non-synaptic mechanisms improve convergence
754 in cell assembly. *Neural Networks: The Official Journal of the International Neural*
755 *Network Society* **122**:420–433. doi:10.1016/j.neunet.2019.09.038
756 DePasquale B, Sussillo D, Abbott LF, Churchland MM. 2023. The centrality of population-level
757 factors to network computation is demonstrated by a versatile approach for training
758 spiking networks. *Neuron* **111**:631-649.e10. doi:10.1016/j.neuron.2022.12.007
759 Dhillon A, Jones RS. 2000. Laminar differences in recurrent excitatory transmission in the rat
760 entorhinal cortex in vitro. *Neuroscience* **99**:413–422. doi:10.1016/s0306-4522(00)00225-
761 6
762 Dyhrfjeld-Johnsen J, Santhakumar V, Morgan RJ, Huerta R, Tsimring L, Soltesz I. 2007.
763 Topological determinants of epileptogenesis in large-scale structural and functional
764 models of the dentate gyrus derived from experimental data. *Journal of neurophysiology*
765 **97**:1566–1587. doi:10.1152/jn.00950.2006
766 Ecker A, Romani A, Sáray S, Káli S, Migliore M, Falck J, Lange S, Mercer A, Thomson AM, Muller
767 E, Reimann MW, Ramaswamy S. 2020. Data-driven integration of hippocampal CA1
768 synaptic physiology in silico. *Hippocampus* **30**:1129–1145. doi:10.1002/hipo.23220
769 Eke DO, Bernard A, Bjaalie JG, Chavarriaga R, Hanakawa T, Hannan AJ, Hill SL, Martone ME,
770 McMahon A, Ruebel O, Crook S, Thiels E, Pestilli F. 2022. International data governance
771 for neuroscience. *Neuron* **110**:600–612. doi:10.1016/j.neuron.2021.11.017
772 Faghihi F, Moustafa AA. 2017. Combined Computational Systems Biology and Computational
773 Neuroscience Approaches Help Develop of Future "Cognitive Developmental Robotics."
774 *Frontiers in Neurorobotics* **11**:63. doi:10.3389/fnbot.2017.00063
775 Ferguson AR, Nielson JL, Cragin MH, Bandrowski AE, Martone ME. 2014. Big data from small
776 data: data-sharing in the "long tail" of neuroscience. *Nature Neuroscience* **17**:1442–
777 1447. doi:10.1038/nn.3838
778 Gastaldi C, Schwalger T, De Falco E, Quiroga RQ, Gerstner W. 2021. When shared concept cells
779 support associations: Theory of overlapping memory engrams. *PLOS Computational*
780 *Biology* **17**:e1009691. doi:10.1371/journal.pcbi.1009691
781 Gleeson P, Davison AP, Silver RA, Ascoli GA. 2017. A Commitment to Open Source in
782 Neuroscience. *Neuron* **96**:964–965. doi:10.1016/j.neuron.2017.10.013
783 Gulyás AI, Freund TF, Káli S. 2016. The Effects of Realistic Synaptic Distribution and 3D
784 Geometry on Signal Integration and Extracellular Field Generation of Hippocampal
785 Pyramidal Cells and Inhibitory Neurons. *Frontiers in Neural Circuits* **10**:88.
786 doi:10.3389/fncir.2016.00088
787 Guzman SJ, Schlögl A, Espinoza C, Zhang X, Suter BA, Jonas P. 2021. How connectivity rules and
788 synaptic properties shape the efficacy of pattern separation in the entorhinal cortex–
789 dentate gyrus–CA3 network. *Nature Computational Science* **1**:830–842.
790 doi:10.1038/s43588-021-00157-1
791 Hamilton DJ, Wheeler DW, White CM, Rees CL, Komendantov AO, Bergamino M, Ascoli GA.
792 2017a. Name-calling in the hippocampus (and beyond): coming to terms with neuron
793 types and properties. *Brain Informatics* **4**:1–12. doi:10.1007/s40708-016-0053-3

Hamilton DJ, White CM, Rees CL, Wheeler DW, Ascoli GA. 2017b. Molecular fingerprinting of principal neurons in the rodent hippocampus: A neuroinformatics approach. *Journal of Pharmaceutical and Biomedical Analysis* **144**:269–278. doi:10.1016/j.jpba.2017.03.062

Hosp JA, Strüber M, Yanagawa Y, Obata K, Vida I, Jonas P, Bartos M. 2014. Morpho-physiological criteria divide dentate gyrus interneurons into classes. *Hippocampus* **24**:189–203. doi:10.1002/hipo.22214

Hunsberger MS, Mynlieff M. 2020. BK potassium currents contribute differently to action potential waveform and firing rate as rat hippocampal neurons mature in the first postnatal week. *Journal of Neurophysiology* **124**:703–714. doi:10.1152/jn.00711.2019

Insel TR, Landis SC, Collins FS. 2013. Research priorities. The NIH BRAIN Initiative. *Science (New York, NY)* **340**:687–688. doi:10.1126/science.1239276

Izhikevich EM. 2003. Simple model of spiking neurons. *IEEE transactions on neural networks* **14**:1569–1572. doi:10.1109/TNN.2003.820440

Jones AR, Overly CC, Sunkin SM. 2009. The Allen Brain Atlas: 5 years and beyond. *Nature Reviews Neuroscience* **10**:821–828. doi:10.1038/nrn2722

Kirson ED, Yaari Y. 2000. Unique properties of NMDA receptors enhance synaptic excitation of radiatum giant cells in rat hippocampus. *The Journal of Neuroscience: The Official Journal of the Society for Neuroscience* **20**:4844–4854.

Knöpfel T, Song C. 2019. Optical voltage imaging in neurons: moving from technology development to practical tool. *Nature Reviews Neuroscience* **20**:719–727. doi:10.1038/s41583-019-0231-4

Kohara K, Pignatelli M, Rivest AJ, Jung H-Y, Kitamura T, Suh J, Frank D, Kajikawa K, Mise N, Obata Y, Wickersham IR, Tonegawa S. 2014. Cell type-specific genetic and optogenetic tools reveal hippocampal CA2 circuits. *Nature Neuroscience* **17**:269–279. doi:10.1038/nn.3614

Komendantov AO, Venkadesh S, Rees CL, Wheeler DW, Hamilton DJ, Ascoli GA. 2019. Quantitative firing pattern phenotyping of hippocampal neuron types. *Scientific Reports* **9**:17915. doi:10.1038/s41598-019-52611-w

Koopmans F, van Nierop P, Andres-Alonso M, Byrnes A, Cijsouw T, Coba MP, Cornelisse LN, Farrell RJ, Goldschmidt HL, Howrigan DP, Hussain NK, Imig C, de Jong APH, Jung H, Kohansalnodehi M, Kramarz B, Lipstein N, Lovering RC, MacGillavry H, Mariano V, Mi H, Ninov M, Osumi-Sutherland D, Pielot R, Smalla KH, Tang H, Tashman K, Toonen RFG, Verpelli C, Reig-Viader R, Watanabe K, van Weering J, Achsel T, Ashrafi G, Asi N, Brown TC, De Camilli P, Feuermann M, Foulger RE, Gaudet P, Joglekar A, Kanellopoulos A, Malenka R, Nicoll RA, Pulido C, de Juan-Sanz J, Sheng M, Südhof TC, Tilgner HU, Bagni C, Bayés À, Biederer T, Brose N, Chua JJE, Dieterich DC, Gundelfinger ED, Hoogenraad C, Huganir RL, Jahn R, Kaeser PS, Kim E, Kreutz MR, McPherson PS, Neale BM, O'Connor V, Posthuma D, Ryan TA, Sala C, Feng G, Hyman SE, Thomas PD, Smit AB, Verhage M. 2019. SynGO: An Evidence-Based, Expert-Curated Knowledge Base for the Synapse. *Neuron* **103**:217-234.e4. doi:10.1016/j.neuron.2019.05.002

Kopsick JD, Tecuatl C, Moradi K, Attili SM, Kashyap HJ, Xing J, Chen K, Krichmar JL, Ascoli GA. 2022. Robust Resting-State Dynamics in a Large-Scale Spiking Neural Network Model of Area CA3 in the Mouse Hippocampus. *Cognitive Computation*. doi:10.1007/s12559-021-09954-2

838 Lee C-T, Kao M-H, Hou W-H, Wei Y-T, Chen C-L, Lien C-C. 2016. Causal Evidence for the Role of
839 Specific GABAergic Interneuron Types in Entorhinal Recruitment of Dentate Granule
840 Cells. *Scientific Reports* **6**:36885. doi:10.1038/srep36885
841 Lee S-H, Marchionni I, Bezaire M, Varga C, Danielson N, Lovett-Barron M, Losonczy A, Soltesz I.
842 2014. Parvalbumin-positive basket cells differentiate among hippocampal pyramidal
843 cells. *Neuron* **82**:1129–44. doi:10.1016/j.neuron.2014.03.034
844 Lein E, Borm LE, Linnarsson S. 2017. The promise of spatial transcriptomics for neuroscience in
845 the era of molecular cell typing. *Science* **358**:64–69. doi:10.1126/science.aan6827
846 Lein ES, Hawrylycz MJ, Ao N, Ayres M, Bensinger A, Bernard A, Boe AF, Boguski MS, Brockway
847 KS, Byrnes EJ, Chen Lin, Chen Li, Chen T-M, Chin MC, Chong J, Crook BE, Czaplinska A,
848 Dang CN, Datta S, Dee NR, Desaki AL, Desta T, Diep E, Dolbeare TA, Donelan MJ, Dong H-
849 W, Dougherty JG, Duncan BJ, Ebbert AJ, Eichele G, Estin LK, Faber C, Facer BA, Fields R,
850 Fischer SR, Fliss TP, Frensley C, Gates SN, Glattfelder KJ, Halverson KR, Hart MR,
851 Hohmann JG, Howell MP, Jeung DP, Johnson RA, Karr PT, Kawal R, Kidney JM, Knapik RH,
852 Kuan CL, Lake JH, Laramee AR, Larsen KD, Lau C, Lemon TA, Liang AJ, Liu Y, Luong LT,
853 Michaels J, Morgan JJ, Morgan RJ, Mortrud MT, Mosqueda NF, Ng LL, Ng R, Orta GJ,
854 Overly CC, Pak TH, Parry SE, Pathak SD, Pearson OC, Puchalski RB, Riley ZL, Rockett HR,
855 Rowland SA, Royall JJ, Ruiz MJ, Sarno NR, Schaffnit K, Shapovalova NV, Sivisay T,
856 Slaughterbeck CR, Smith SC, Smith KA, Smith BI, Sodt AJ, Stewart NN, Stumpf K-R, Sunkin
857 SM, Sutram M, Tam A, Teemer CD, Thaller C, Thompson CL, Varnam LR, Visel A, Whitlock
858 RM, Wohnoutka PE, Wolkey CK, Wong VY, Wood M, Yaylaoglu MB, Young RC,
859 Youngstrom BL, Yuan XF, Zhang B, Zwingman TA, Jones AR. 2007. Genome-wide atlas of
860 gene expression in the adult mouse brain. *Nature* **445**:168–176.
861 doi:10.1038/nature05453
862 Li XG, Somogyi P, Ylinen A, Buzsáki G. 1994. The hippocampal CA3 network: an in vivo
863 intracellular labeling study. *The Journal of Comparative Neurology* **339**:181–208.
864 doi:10.1002/cne.903390204
865 Lopez-Rojas J, de Solis CA, Leroy F, Kandel ER, Siegelbaum SA. 2022. A direct lateral entorhinal
866 cortex to hippocampal CA2 circuit conveys social information required for social
867 memory. *Neuron* **110**:1559-1572.e4. doi:10.1016/j.neuron.2022.01.028
868 Lübke J, Frotscher M, Spruston N. 1998. Specialized electrophysiological properties of
869 anatomically identified neurons in the hilar region of the rat fascia dentata. *Journal of*
870 *Neurophysiology* **79**:1518–1534. doi:10.1152/jn.1998.79.3.1518
871 Luo Y-F, Ye X-X, Fang Y-Z, Li M-D, Xia Z-X, Liu J-M, Lin X-S, Huang Z, Zhu X-Q, Huang J-J, Tan D-L,
872 Zhang Y-F, Liu H-P, Zhou J, Shen Z-C. 2021. mTORC1 Signaling Pathway Mediates Chronic
873 Stress-Induced Synapse Loss in the Hippocampus. *Frontiers in Pharmacology* **12**:801234.
874 doi:10.3389/fphar.2021.801234
875 Markram H. 2006. The blue brain project. *Nature Reviews Neuroscience* **7**:153–160.
876 doi:10.1038/nrn1848
877 Markwardt SJ, Dieni CV, Wadiche JI, Overstreet-Wadiche L. 2011. Ivy/neurogliaform
878 interneurons coordinate activity in the neurogenic niche. *Nature Neuroscience* **14**:1407–
879 1409. doi:10.1038/nn.2935
880 McDougal RA, Morse TM, Carnevale T, Marenco L, Wang R, Migliore M, Miller PL, Shepherd
881 GM, Hines ML. 2017. Twenty years of ModelDB and beyond: building essential modeling

tools for the future of neuroscience. *Journal of Computational Neuroscience* **42**:1–10. doi:10.1007/s10827-016-0623-7

Mehta K, Goldin RF, Marchette D, Vogelstein JT, Priebe CE, Ascoli GA. 2021. Neuronal classification from network connectivity via adjacency spectral embedding. *Network Neuroscience (Cambridge, Mass)* **5**:689–710. doi:10.1162/netn_a_00195

Migliore R, Lupascu CA, Bologna LL, Romani A, Courcol J-D, Antonel S, Van Geit WAH, Thomson AM, Mercer A, Lange S, Falck J, Rössert CA, Shi Y, Hagens O, Pezzoli M, Freund TF, Kali S, Muller EB, Schürmann F, Markram H, Migliore M. 2018. The physiological variability of channel density in hippocampal CA1 pyramidal cells and interneurons explored using a unified data-driven modeling workflow. *PLOS Computational Biology* **14**:e1006423. doi:10.1371/journal.pcbi.1006423

Moradi K, Aldarraji Z, Luthra M, Madison GP, Ascoli GA. 2022. Normalized unitary synaptic signaling of the hippocampus and entorhinal cortex predicted by deep learning of experimental recordings. *Communications Biology* **5**:418. doi:10.1038/s42003-022-03329-5

Moradi K, Ascoli GA. 2020. A comprehensive knowledge base of synaptic electrophysiology in the rodent hippocampal formation. *Hippocampus* **30**:314–331. doi:10.1002/hipo.23148

Moradi K, Ascoli GA. 2018. Systematic Data Mining of Hippocampal Synaptic Properties In: Cutsuridis V, Graham BP, Cobb S, Vida I, editors. Hippocampal Microcircuits, Springer Series in Computational Neuroscience. Cham: Springer International Publishing. pp. 441–471. doi:10.1007/978-3-319-99103-0_11

Muñoz-Castañeda R, Zingg B, Matho KS, Chen X, Wang Q, Foster NN, Li A, Narasimhan A, Hirokawa KE, Huo B, Bannerjee S, Korobkova L, Park CS, Park Y-G, Bienkowski MS, Chon U, Wheeler DW, Li Xiangning, Wang Yun, Naeemi M, Xie P, Liu L, Kelly K, An X, Attili SM, Bowman I, Bludova A, Cetin A, Ding L, Drewes R, D'Orazi F, Elowsky C, Fischer S, Galbavy W, Gao L, Gillis J, Groblewski PA, Gou L, Hahn JD, Hatfield JT, Hintiryan H, Huang JJ, Kondo H, Kuang X, Lesnar P, Li Xu, Li Y, Lin M, Lo D, Mizrachi J, Mok S, Nicovich PR, Palaniswamy R, Palmer J, Qi X, Shen E, Sun Y-C, Tao HW, Wakemen W, Wang Yimin, Yao S, Yuan J, Zhan H, Zhu M, Ng L, Zhang LI, Lim BK, Hawrylycz M, Gong H, Gee JC, Kim Y, Chung K, Yang XW, Peng H, Luo Q, Mitra PP, Zador AM, Zeng H, Ascoli GA, Josh Huang Z, Osten P, Harris JA, Dong H-W. 2021. Cellular anatomy of the mouse primary motor cortex. *Nature* **598**:159–166. doi:10.1038/s41586-021-03970-w

Nageswaran JM, Dutt N, Krichmar JL, Nicolau A, Veidenbaum AV. 2009. A configurable simulation environment for the efficient simulation of large-scale spiking neural networks on graphics processors. *Neural Networks: The Official Journal of the International Neural Network Society* **22**:791–800. doi:10.1016/j.neunet.2009.06.028

Navas-Olive A, Valero M, Jurado-Parras T, de Salas-Quiroga A, Averkin RG, Gambino G, Cid E, de la Prida LM. 2020. Multimodal determinants of phase-locked dynamics across deep-superficial hippocampal sublayers during theta oscillations. *Nature Communications* **11**:2217. doi:10.1038/s41467-020-15840-6

Niedermeier L, Chen K, Xing J, Das A, Kopsick J, Scott E, Sutton N, Weber K, Dutt N, Krichmar JL. 2022. CARLsim 6: An Open Source Library for Large-Scale, Biologically Detailed Spiking Neural Network Simulation2022 International Joint Conference on Neural Networks

(IJCNN). Presented at the 2022 International Joint Conference on Neural Networks (IJCNN). Padua, Italy: IEEE. pp. 1–10. doi:10.1109/IJCNN55064.2022.9892644

Obafemi TO, Owolabi OV, Omiyale BO, Afolabi BA, Ojo OA, Onasanya A, Adu IAI, Rotimi D. 2021. Combination of donepezil and gallic acid improves antioxidant status and cholinesterases activity in aluminum chloride-induced neurotoxicity in Wistar rats. *Metabolic Brain Disease* **36**:2511–2519. doi:10.1007/s11011-021-00749-w

Petilla Interneuron Nomenclature Group, Ascoli GA, Alonso-Nanclares L, Anderson SA, Barrionuevo G, Benavides-Piccione R, Burkhalter A, Buzsáki G, Cauli B, Defelipe J, Fairén A, Feldmeyer D, Fishell G, Fregnac Y, Freund TF, Gardner D, Gardner EP, Goldberg JH, Helmstaedter M, Hestrin S, Karube F, Kisvárday ZF, Lambolez B, Lewis DA, Marin O, Markram H, Muñoz A, Packer A, Petersen CCH, Rockland KS, Rossier J, Rudy B, Somogyi P, Staiger JF, Tamas G, Thomson AM, Toledo-Rodriguez M, Wang Y, West DC, Yuste R. 2008. Petilla terminology: nomenclature of features of GABAergic interneurons of the cerebral cortex. *Nature Reviews Neuroscience* **9**:557–568. doi:10.1038/nrn2402

Puighermanal E, Cutando L, Boubaker-Vitre J, Honoré E, Longueville S, Hervé D, Valjent E. 2017. Anatomical and molecular characterization of dopamine D1 receptor-expressing neurons of the mouse CA1 dorsal hippocampus. *Brain Structure & Function* **222**:1897–1911. doi:10.1007/s00429-016-1314-x

Rees CL, Moradi K, Ascoli GA. 2017. Weighing the Evidence in Peters' Rule: Does Neuronal Morphology Predict Connectivity?, Trends in Neurosciences. Elsevier Ltd. doi:10.1016/j.tins.2016.11.007

Rees CL, Wheeler DW, Hamilton DJ, White CM, Komendantov AO, Ascoli GA. 2016. Graph theoretic and motif analyses of the hippocampal neuron type potential connectome. *eNeuro* **3**. doi:10.1523/ENEURO.0205-16.2016

Romani A, Antonietti A, Bella D, Budd J, Giacalone E, Kurban K, Sáray S, Abdellah M, Arnaudon A, Boci E, Colangelo C, Courcol J-D, Delemontex T, Ecker A, Falck J, Favreau C, Gevaert M, Hernando JB, Herttuainen J, Ivaska G, Kanari L, Kaufmann A-K, King JG, Kumbhar P, Lange S, Lu H, Lupascu CA, Migliore R, Petitjean F, Planas J, Rai P, Ramaswamy S, Reimann MW, Riquelme JL, Guerrero NR, Shi Y, Sood V, Sy MF, Geit WV, Vanherpe L, Freund TF, Mercer A, Muller E, Schürmann F, Thomson AM, Migliore M, Káli S, Markram H. 2023. Community-based Reconstruction and Simulation of a Full-scale Model of Region CA1 of Rat Hippocampus (preprint). Neuroscience. doi:10.1101/2023.05.17.541167

Ropireddy D, Scorcioni R, Lasher B, Buzsáki G, Ascoli GA. 2011. Axonal morphometry of hippocampal pyramidal neurons semi-automatically reconstructed after in vivo labeling in different CA3 locations. *Brain Structure & Function* **216**:1–15. doi:10.1007/s00429-010-0291-8

Sanchez-Aguilera A, Wheeler DW, Jurado-Parras T, Valero M, Nokia MS, Cid E, Fernandez-Lamo I, Sutton N, García-Rincón D, de la Prida LM, Ascoli GA. 2021. An update to Hippocampome.org by integrating single-cell phenotypes with circuit function in vivo. *PLoS Biology* **19**:e3001213. doi:10.1371/journal.pbio.3001213

Sáray S, Rössert CA, Appukuttan S, Migliore R, Vitale P, Lupascu CA, Bologna LL, Van Geit W, Romani A, Davison AP, Muller E, Freund TF, Káli S. 2021. HippoUnit: A software tool for the automated testing and systematic comparison of detailed models of hippocampal

969 neurons based on electrophysiological data. *PLoS computational biology* **17**:e1008114.
970 doi:10.1371/journal.pcbi.1008114
971 Sargolini F, Fyhn M, Hafting T, McNaughton BL, Witter MP, Moser M-B, Moser EI. 2006.
972 Conjunctive representation of position, direction, and velocity in entorhinal cortex.
973 *Science (New York, NY)* **312**:758–762. doi:10.1126/science.1125572
974 Savanthrapadian S, Meyer T, Elgueta C, Booker SA, Vida I, Bartos M. 2014. Synaptic properties
975 of SOM- and CCK-expressing cells in dentate gyrus interneuron networks. *The Journal of*
976 *Neuroscience: The Official Journal of the Society for Neuroscience* **34**:8197–8209.
977 doi:10.1523/JNEUROSCI.5433-13.2014
978 Schumm SN, Gabrieli D, Meaney DF. 2022. Plasticity impairment exposes CA3 vulnerability in a
979 hippocampal network model of mild traumatic brain injury. *Hippocampus* **32**:231–250.
980 doi:10.1002/hipo.23402
981 Schumm SN, Gabrieli D, Meaney DF. 2020. Neuronal Degeneration Impairs Rhythms Between
982 Connected Microcircuits. *Frontiers in Computational Neuroscience* **14**:18.
983 doi:10.3389/fncom.2020.00018
984 Scorcioni R, Polavaram S, Ascoli GA. 2008. L-Measure: a web-accessible tool for the analysis,
985 comparison and search of digital reconstructions of neuronal morphologies. *Nature*
986 *Protocols* **3**:866–876. doi:10.1038/nprot.2008.51
987 Shepherd GM, Marenco L, Hines ML, Migliore M, McDougal RA, Carnevale NT, Newton AJH,
988 Surles-Zeigler M, Ascoli GA. 2019. Neuron Names: A Gene- and Property-Based Name
989 Format, With Special Reference to Cortical Neurons. *Frontiers in Neuroanatomy* **13**:25.
990 doi:10.3389/fnana.2019.00025
991 Sik A, Tamamaki N, Freund TF. 1993. Complete axon arborization of a single CA3 pyramidal cell
992 in the rat hippocampus, and its relationship with postsynaptic parvalbumin-containing
993 interneurons. *The European journal of neuroscience* **5**:1719–28.
994 Skene NG, Grant SGN. 2016. Identification of Vulnerable Cell Types in Major Brain Disorders
995 Using Single Cell Transcriptomes and Expression Weighted Cell Type Enrichment.
996 *Frontiers in Neuroscience* **10**:16. doi:10.3389/fnins.2016.00016
997 Smith JH, Rowland C, Harland B, Moslehi S, Montgomery RD, Schobert K, Watterson WJ,
998 Dalrymple-Alford J, Taylor RP. 2021. How neurons exploit fractal geometry to optimize
999 their network connectivity. *Scientific Reports* **11**:2332. doi:10.1038/s41598-021-81421-2
1000 Stein L, Sternberg P, Durbin R, Thierry-Mieg J, Spieth J. 2001. WormBase: network access to the
1001 genome and biology of Caenorhabditis elegans. *Nucleic Acids Research* **29**:82–86.
1002 doi:10.1093/nar/29.1.82
1003 Steward O. 1976. Topographic organization of the projections from the entorhinal area to the
1004 hippocampal formation of the rat. *The Journal of Comparative Neurology* **167**:285–314.
1005 doi:10.1002/cne.901670303
1006 Sutton NM, Ascoli GA. 2021. Spiking Neural Networks and Hippocampal Function: A Web-
1007 Accessible Survey of Simulations, Modeling Methods, and Underlying Theories.
1008 *Cognitive Systems Research* **70**:80–92. doi:10.1016/j.cogsys.2021.07.008
1009 Szabadics J, Soltesz I. 2009. Functional specificity of mossy fiber innervation of GABAergic cells
1010 in the hippocampus. *The Journal of Neuroscience: The Official Journal of the Society for*
1011 *Neuroscience* **29**:4239–4251. doi:10.1523/JNEUROSCI.5390-08.2009

Takács VT, Klausberger T, Somogyi P, Freund TF, Gulyás AI. 2012. Extrinsic and local glutamatergic inputs of the rat hippocampal CA1 area differentially innervate pyramidal cells and interneurons. *Hippocampus* **22**:1379–1391. doi:10.1002/hipo.20974

Tecuatl C, Wheeler DW, Ascoli GA. 2021a. A Method for Estimating the Potential Synaptic Connections Between Axons and Dendrites From 2D Neuronal Images. *Bio-Protocol* **11**:e4073. doi:10.21769/BioProtoc.4073

Tecuatl C, Wheeler DW, Sutton N, Ascoli GA. 2021b. Comprehensive Estimates of Potential Synaptic Connections in Local Circuits of the Rodent Hippocampal Formation by Axonal-Dendritic Overlap. *The Journal of Neuroscience: The Official Journal of the Society for Neuroscience* **41**:1665–1683. doi:10.1523/JNEUROSCI.1193-20.2020

The FlyBase Consortium. 1994. FlyBase--the Drosophila database. *Nucleic Acids Research* **22**:3456–3458. doi:10.1093/nar/22.17.3456

Tsodyks M, Pawelzik K, Markram H. 1998. Neural networks with dynamic synapses. *Neural Computation* **10**:821–835. doi:10.1162/089976698300017502

Vaden RJ, Gonzalez JC, Tsai M-C, Niver AJ, Fusilier AR, Griffith CM, Kramer RH, Wadiche JI, Overstreet-Wadiche L. 2020. Parvalbumin interneurons provide spillover to newborn and mature dentate granule cells. *eLife* **9**:e54125. doi:10.7554/eLife.54125

Valero M, Cid E, Averkin RG, Aguilar J, Sanchez-Aguilera A, Viney TJ, Gomez-Dominguez D, Bellistri E, de la Prida LM. 2015. Determinants of different deep and superficial CA1 pyramidal cell dynamics during sharp-wave ripples. *Nature Neuroscience* **18**:1281–1290. doi:10.1038/nn.4074

Venkadesh S, Komendantov AO, Listopad S, Scott EO, De Jong K, Krichmar JL, Ascoli GA. 2018. Evolving Simple Models of Diverse Intrinsic Dynamics in Hippocampal Neuron Types. *Frontiers in Neuroinformatics* **12**:8. doi:10.3389/fninf.2018.00008

Venkadesh S, Komendantov AO, Wheeler DW, Hamilton DJ, Ascoli GA. 2019. Simple models of quantitative firing phenotypes in hippocampal neurons: Comprehensive coverage of intrinsic diversity. *PLOS Computational Biology* **15**:e1007462. doi:10.1371/journal.pcbi.1007462

Venkadesh S, Van Horn JD. 2021. Integrative Models of Brain Structure and Dynamics: Concepts, Challenges, and Methods. *Frontiers in Neuroscience* **15**:752332. doi:10.3389/fnins.2021.752332

Walker AS, Raliski BK, Nguyen DV, Zhang P, Sanders K, Karbasi K, Miller EW. 2021. Imaging Voltage in Complete Neuronal Networks Within Patterned Microislands Reveals Preferential Wiring of Excitatory Hippocampal Neurons. *Frontiers in Neuroscience* **15**:643868. doi:10.3389/fnins.2021.643868

Wheeler DW, White CM, Rees CL, Komendantov AO, Hamilton DJ, Ascoli GA. 2015. Hippocampome.org: a knowledge base of neuron types in the rodent hippocampus. *eLife* **4**. doi:10.7554/eLife.09960

White CM, Rees CL, Wheeler DW, Hamilton DJ, Ascoli GA. 2020. Molecular expression profiles of morphologically defined hippocampal neuron types: Empirical evidence and relational inferences. *Hippocampus* **30**:472–487. doi:10.1002/hipo.23165

Winnubst J, Bas E, Ferreira TA, Wu Z, Economo MN, Edson P, Arthur BJ, Bruns C, Rokicki K, Schauder D, Olbris DJ, Murphy SD, Ackerman DG, Arshadi C, Baldwin P, Blake R, Elsayed A, Hasan M, Ramirez D, Dos Santos B, Weldon M, Zafar A, Dudman JT, Gerfen CR,

Hantman AW, Korff W, Sternson SM, Spruston N, Svoboda K, Chandrashekar J. 2019. Reconstruction of 1,000 Projection Neurons Reveals New Cell Types and Organization of Long-Range Connectivity in the Mouse Brain. *Cell* **179**:268-281.e13. doi:10.1016/j.cell.2019.07.042

Winnubst J, Spruston N, Harris JA. 2020. Linking axon morphology to gene expression: a strategy for neuronal cell-type classification. *Current Opinion in Neurobiology* **65**:70–76. doi:10.1016/j.conb.2020.10.006

Wittner L, Henze DA, Záborszky L, Buzsáki G. 2007. Three-dimensional reconstruction of the axon arbor of a CA3 pyramidal cell recorded and filled in vivo. *Brain Structure & Function* **212**:75–83. doi:10.1007/s00429-007-0148-y

Wynne ME, Lane AR, Singleton KS, Zlatic SA, Gokhale A, Werner E, Duong D, Kwong JQ, Crocker AJ, Faundez V. 2021. Heterogeneous Expression of Nuclear Encoded Mitochondrial Genes Distinguishes Inhibitory and Excitatory Neurons. *eNeuro* **8**:ENEURO.0232-21.2021. doi:10.1523/ENEURO.0232-21.2021

Yao Z, Van Velthoven CTJ, Nguyen TN, Goldy J, Sedeno-Cortes AE, Baftizadeh F, Bertagnolli D, Casper T, Chiang M, Crichton K, Ding S-L, Fong O, Garren E, Glandon A, Gouwens NW, Gray J, Graybuck LT, Hawrylycz MJ, Hirschstein D, Kroll M, Lathia K, Lee C, Levi B, McMillen D, Mok S, Pham T, Ren Q, Rimorin C, Shapovalova N, Sulc J, Sunkin SM, Tieu M, Torkelson A, Tung H, Ward K, Dee N, Smith KA, Tasic B, Zeng H. 2021. A taxonomy of transcriptomic cell types across the isocortex and hippocampal formation. *Cell* **184**:3222-3241.e26. doi:10.1016/j.cell.2021.04.021

Yeung AWK, Goto TK, Leung WK. 2017. The Changing Landscape of Neuroscience Research, 2006-2015: A Bibliometric Study. *Frontiers in Neuroscience* **11**:120. doi:10.3389/fnins.2017.00120

Yuste R, Hawrylycz M, Aalling N, Aguilar-Valles A, Arendt D, Armañanzas R, Ascoli GA, Bielza C, Bokharaie V, Bergmann TB, Bystron I, Capogna M, Chang Y, Clemens A, de Kock CPJ, DeFelipe J, Dos Santos SE, Dunville K, Feldmeyer D, Fiáth R, Fishell GJ, Foggetti A, Gao X, Ghaderi P, Goriounova NA, Güntürkün O, Hagihara K, Hall VJ, Helmstaedter M, Herculano-Houzel S, Hilscher MM, Hirase H, Hjerling-Leffler J, Hodge R, Huang J, Huda R, Khodosevich K, Kiehn O, Koch H, Kuebler ES, Kühnemund M, Larrañaga P, Lelieveldt B, Louth EL, Lui JH, Mansvelder HD, Marin O, Martinez-Trujillo J, Chameh HM, Mohapatra AN, Munguba H, Nedergaard M, Němec P, Ofer N, Pfisterer UG, Pontes S, Redmond W, Rossier J, Sanes JR, Scheuermann RH, Serrano-Saiz E, Staiger JF, Somogyi P, Tamás G, Tolias AS, Tosches MA, García MT, Wozny C, Wuttke TV, Liu Y, Yuan J, Zeng H, Lein E. 2020. A community-based transcriptomics classification and nomenclature of neocortical cell types. *Nature Neuroscience* **23**:1456–1468. doi:10.1038/s41593-020-0685-8

Zagrean A-M, Georgescu I-A, Iesanu MI, Ionescu R-B, Haret RM, Panaitescu AM, Zagrean L. 2022. Oxytocin and vasopressin in the hippocampus. *Vitamins and Hormones* **118**:83–127. doi:10.1016/bs.vh.2021.11.002

Zeisel A, Muñoz-Manchado AB, Codeluppi S, Lönnerberg P, Manno GL, Juréus A, Marques S, Munguba H, He L, Betsholtz C, Rolny C, Castelo-Branco G, Hjerling-Leffler J, Linnarsson S. 2015. Cell types in the mouse cortex and hippocampus revealed by single-cell RNA-seq. *Science* **347**:1138–1142. doi:10.1126/science.aaa1934

1100 Zeng H, Sanes JR. 2017. Neuronal cell-type classification: challenges, opportunities and the path
1101 forward. *Nature Reviews Neuroscience* **18**:530–546. doi:10.1038/nrn.2017.85
1102 Zilli EA. 2012. Models of grid cell spatial firing published 2005-2011. *Frontiers in Neural Circuits*
1103 **6**:16. doi:10.3389/fncir.2012.00016
1104
1105

1106 **Tables**

1107

1108 **Table 1. Added knowledge and functioning in Hippocampome.org releases v1.1-12.**

1109

Version	Contribution	Article
v1.1	• definitions for terms and phrases relevant to Hippocampome.org	(Hamilton et al., 2017a)
v1.2	• clickable connectivity matrix • interactive connectivity navigator Java applet • searching by connectivity	(Rees et al., 2016)
v1.3	• downloadable list of ABA predictions of marker expressions • utility for viewing the effects of thresholds on ABA marker expression predictions	(Hamilton et al., 2017b)
v1.4	• access to the synapse knowledge base	(Moradi and Ascoli, 2020)
v1.5	• relational biomarker expression inferences	(White et al., 2020)
v1.6	• firing pattern phenotypes • clickable firing pattern matrix • clickable firing pattern parameters matrix • search by firing pattern • search by firing pattern parameter	(Komendantov et al., 2019)
v1.7	• Izhikevich models • clickable Izhikevich model parameters matrix • downloadable single-neuron parameter files • downloadable single-neuron CARLSim4 simulation files • ability to perform single-neuron simulations of the firing patterns	(Venkadesh et al., 2019)
v1.8	• clickable/downloadable neurite lengths matrix • clickable/downloadable somatic path distances matrix • clickable/downloadable numbers of potential synapses matrix • clickable/downloadable numbers of contacts matrix • clickable/downloadable connection probabilities matrix	(Tecuatl et al., 2021b)
v1.9	• clickable matrix for *in vivo* recordings	(Sanchez-Aguilera et al., 2021)
v1.10	• Cognome knowledge base of spiking neural circuit functions and network simulations of the hippocampal formation	(Sutton and Ascoli, 2021)
v1.11	• clickable matrix of neuron type census values for rat and mouse	(Attili et al., 2022)
v1.12	• clickable/downloadable matrices of synaptic physiology parameter values (g, τ_d, τ_r, τ_f, U) for combinations of species, sex, age, temperature, and recording mode	(Moradi et al., 2022)

1110

1111 **Table 2.** Probabilities of connection and number of contacts per connected pair from DG
1112 Granule cell to mossy fibers targets in CA3.
1113

Postsynaptic neuron type	Probability	# contacts
CA3 Pyramidal	1.11E-04	1.08
CA3c Pyramidal	3.91E-04	1.31
CA3 Spiny Lucidum Dentate-Projecting	5.89E-04	1.69
CA3 Mossy Fiber-Associated ORDEN	4.44E-04	1.27
CA3 Basket	6.55E-04	1.50
CA3 Basket CCK+	2.14E-04	1.16
CA3 Ivy	3.35E-04	1.29
CA3 Mossy Fiber-Associated	3.78E-05	1.04
CA3 LMR-Targeting	1.31E-04	1.21
CA3 Lucidum ORAX	2.62E-04	1.19
CA3 Lucidum-Radiatum	3.25E-04	1.13
CA3 Axo-Axonic	7.56E-04	1.50
CA3 Bistratified	8.25E-04	1.45
CA3 QuadD-LM	2.91E-04	1.25

1114
1115

1116 **Table 3. Examples of independent studies utilizing unique neuronal properties from**
1117 **Hippocampome.org v1.0.**
1118

Article	Usage
(Gulyás et al., 2016)	Lists of subthreshold physiological properties for multicompartmental modeling
(Skene and Grant, 2016)	Catalog of CA1 Interneuron types
(Faghihi and Moustafa, 2017)	Diversity of hippocampal neuron types and morphological neuronal features
(Puighermanal et al., 2017)	Biomarker expression in CA1 interneurons
(Depannemaecker et al., 2020)	Parameter values for a model of synaptic neurotransmission
(Ecker et al., 2020)	Evidence that CA1 interneurons express multiple overlapping chemical markers
(Hunsberger and Mynlieff, 2020)	Cell identification based on firing properties
(Schumm et al., 2020)	Directionality of connections in the hippocampus
(Aery Jones et al., 2021)	Local connectivity of CA1 PV+ interneurons
(Ciarpella et al., 2021)	Lists of hippocampal genes
(Luo et al., 2021)	Confirmation of multiple hippocampal neuron types
(Mehta et al., 2021)	Connectome model inspired by entorhinal-CA1 circuit
(Obafemi et al., 2021)	Principal channels of information processing are DG Granule cells and CA1-3 Pyramidal cells
(Sáray et al., 2021)	Membrane biophysics values for CA1 Pyramidal cells
(Smith et al., 2021)	Omni-directionality of axons of CA1 Pyramidal cells
(Venkadesh and Van Horn, 2021)	Example of a brain region's mesoscopic structural connectivity
(Walker et al., 2021)	Reference to morphological and molecular characteristics of hippocampal principal cells and interneurons
(Wynne et al., 2021)	Example brain region with a variety of cell types
(Kopsick et al., 2022)	Utilize accumulated knowledge as the basis for simulations
(Schumm et al., 2022)	Hippocampal morphology, biomarker expression, connectivity, and typing of neurons
(Zagrean et al., 2022)	Diversity of hippocampal neuronal types and their properties

1119

1120 **Figure Legends**
1121
1122 **Figure 1.** Defining neuron types in Hippocampome.org. A) Properties of a Hippocampome.org v1.0
1123 neuron type. A1) Morphology of a Dentate Gyrus (i)2232 Basket cell (NeuroMorpho.Org cell
1124 NMO_34300: Hosp et al., 2014) with axons (red) in *stratum granulosum* (SG) and dendrites (blue) in all
1125 four layers. A2) Schematic interpretation of the morphological tracing, where the circle represents the
1126 location of the soma in SG, the red triangle the location of the axons in SG, and the blue rectangles the
1127 locations of the dendrites in all four layers. A3) Hippocampome.org representation of the morphology,
1128 where a blue square with a vertical line (|) indicates dendritic presence in the outer two-thirds of the
1129 *stratum moleculare* (SMo) and the inner one-third of the *stratum moleculare* (SMi) and the hilus (H), a
1130 purple square with a cross (+) indicates both axonal and dendritic presence in SG, and a black dot (•)
1131 indicates the soma location in SG. A4) Hippocampome.org numerical coding of the reconstructed
1132 neuron, where 2 indicates the presence of dendrites (in SMo, SMi, and H); and 3 indicates the presence
1133 of both axons and dendrites (in SG). A5) Biomarker expressions, where a green triangle indicates
1134 positive expression for parvalbumin (PV), and blue triangles indicate negative expression for
1135 cholecystokinin (CCK) and vasoactive intestinal polypeptide (VIP). A6) Firing pattern phenotype (non-
1136 adapting spiking (NASP); adapted from Figure 1B1 in Savanthrapadian et al., 2014). A7) Membrane
1137 biophysics values (from Figure 3C and Table 1 in Lübke et al., 1998) recorded at 35-37 °C. B) Properties
1138 for a Hippocampome.org v2.0 neuron type. B1) Morphology of a DG (i)2210 Basket GRALDEN
1139 (NeuroMorpho.Org cell NMO_146159: Vaden et al., 2020) with red axons in SG and blue dendrites in
1140 SMo and Smi. B2) Schematic interpretation of the reconstruction (same symbols as in A2). B3-4)
1141 Hippocampome.org representation and numerical coding of the morphology (same symbols as in A3-4).
1142 B5) Biomarker expression. B6) Firing pattern phenotype (silence preceded by transient stuttering
1143 (TSTUT.SLN); adapted from Figure S4 in Markwardt et al., 2011). B7) Membrane biophysics values
1144 recorded at room temperature (from Figure 4D in Vaden et al., 2020), and at 22 °C (from Figure S4 in
1145 Markwardt et al., 2011); emboldened values were extracted from the firing pattern trace in B6.
1146 Membrane biophysics abbreviations: V_{rest}: resting membrane potential; V_{thresh}: firing threshold potential;
1147 AP_{ampl}: action potential amplitude; AP_{width}: action potential width; R_{in}: input resistance; τ_m: membrane
1148 time constant; Max FR: maximum firing rate; fAHP: fast after-hyperpolarizing potential; sAHP: slow
1149 after-hyperpolarizing potential; Sag ratio: ratio of the steady-state membrane potential to the minimum
1150 membrane potential.
1151
1152 **Figure 2.** New neuron types added to Hippocampome.org v2.0. A) Morphology encodings of the 56 new
1153 neuron types that extend the 124 types in Hippocampome.org v1.12. (Left) Increase in number of
1154 neuron types for each subregion. For the neuron type names, excitatory types (e) are in black font and
1155 inhibitory types (i) are in gray font. The 3-6 digit numbers encode the patterns of axons and dendrites in
1156 the layers of the home subregion of the neuron type: 0 = no axons or dendrites, 1 = only axons, 2 = only
1157 dendrites, 3 = both axons and dendrites. A "p" indicates that the neuron types projects across into other
1158 subregions. B) Biomarker expressions of the neuron types. C) Membrane biophysics values for the
1159 neuron types. Morphology abbreviations: DG: dentate gyrus; SMo: outer two-thirds of *stratum*
1160 *moleculare*; SMi: inner one-third of *stratum moleculare*; SG: *stratum granulosum*; H: hilus; SLM: *stratum*
1161 *lacunosum-moleculare*; SR: *stratum radiatum*; SL: *stratum lucidum*; SP: *stratum pyramidale*; SO: *stratum*
1162 *oriens*; Sub: subiculum; PL: polymorphic layer; EC: entorhinal cortex. Marker abbreviations: CB:
1163 calbindin; CR: calretinin; PV: parvalbumin; 5HT-3: serotonin receptor 3; CB1: cannabinoid receptor type
1164 1; GABAa α1: GABA-a alpha 1 subunit; mGluR1a: metabotropic glutamate receptor 1 alpha; Mus2R:
1165 muscarinic type 2 receptor; vGluT3: vesicular glutamate transporter 3; CCK: cholecystokinin; ENK:

enkephalin; NPY: neuropeptide Y; SOM: somatostatin; VIP: vasoactive intestinal polypeptide; nNOS: neuronal nitric oxide synthase; RLN: reelin. Membrane biophysics abbreviations: see Figure 1.

Figure 3. Extensions to the neuronal properties of Hippocampome.org v1.x. A1) Additions to the axonal projections (circled in green) for two v1.0 neuron types. A2) Evidence for the axonal extensions in strata oriens, pyramidale, and radiatum from A1 are circled in green (adapted from Figure 2b in Deller et al., 1996). Scale bar: 75 µm. B1) Biomarker expressions for the two CA1 Pyramidal sub-types added in Hippocampome.org v1.9 (Sanchez-Aguilera et al., 2021). B2) Membrane biophysics values for the two sub-types. B3) CA2 projects preferentially to the deep sublayer of CA1 (Kohara et al., 2014). More perisomatic parvalbumin-positive (PV+) GABAergic boutons are found at CA1 Deep Pyramidal cells (Valero et al., 2015). CA1 Superficial Pyramidal cells form more frequent connections to PV+ CA1 Basket cells, and PV+ CA1 Basket cells form significantly more perisomatic axon terminals on CA1 Deep Pyramidal cells (Lee et al., 2014). C1) Additions to the firing pattern phenotypes of v1.0 neuron types. C2a) Example of adapting spiking (ASP.) in a CA1 Oriens-Bistratified cell (adapted from Figure 4B in Craig and McBain, 2015). C2b) Example of non-adapting spiking (NASP) in a CA3 Basket CCK+ cell (adapted from Figure 3A in Szabadics and Soltesz, 2009). C2c) Example of transient stuttering (TSTUT.) in a CA1 Radiatum Giant cell (adapted from Figure 2Bb in Kirson and Yaari, 2000). C2d) Example of transient stuttering followed by persistent stuttering (TSTUT.PSTUT) in a CA1 Interneuron Specific O-targeting QuadD (adapted from Figure 2D in Chamberland et al., 2010). C2e) Example of silence preceded by transient stuttering (TSTUT.SLN) in a DG MOLAX cell (adapted from Figure S2c in Lee et al., 2016). D) Synaptic probabilities for projecting connections and the corresponding number of contacts in brackets between the two CA3 Pyramidal neuron types and a selection of CA1 neuron types. Morphology abbreviations: see Figure 2. Marker abbreviations: CB: calbindin; Astn2: astrotactin 2; Dcn: decorin; Gpc3: glypican 3; Grp: gastrin releasing peptide; Htr2c: 5-hydroxytryptamine receptor 2c; Ndst4: N-deacetylase and N-sulfotransferase 4; Nov: nephroblastoma overexpressed; Nr3c2: nuclear receptor subfamily 3 group C member 2; Nr4a1: nuclear receptor subfamily 4 group A member 1; Prss12: serine protease 12; Prss23: serine protease 23; Wfs1: wolframin ER transmembrane glycoprotein. Membrane biophysics abbreviations: see Figure 1.

Figure 4. Trends in Hippocampome.org data, knowledge, citations, and usage since v1.0. A) Increase in pieces of knowledge (blue) and evidence (red) with Hippocampome.org version number. B) Number of citations, in which the publication is simply referenced (blue and gray portions), and usage cases, in which the citing work makes use of the information contained within the Hippocampome.org-related work (orange and yellow portions), by year.

Figure 5. Transitional knowledge enabling Hippocampome.org to support spiking neural network simulations. Center: General diagram of the hippocampal formation and the number of cell types in Hippocampome v1.0. A) Neuron type census. Top: General pipeline for obtaining cell counts for specific collections of neurons from the peer reviewed literature. Left: Neuron count proportions for the different subregions of the hippocampal formation. Insert: Normalized neuron counts for the inhibitory vs. excitatory balance by subregion. Right: Neuron counts for five identified CA2 neuron types (green schematic: excitatory, red schematic: inhibitory). B) Neuron dynamics. Top: General pipeline for obtaining Izhikevich models to reproduce the firing pattern phenotypes from peer reviewed data. Right: Simulated firing pattern from a Sub CA1-Projecting Pyramidal cell in response to a 250-pA current injection pulse lasting 1 s. Izhikevich model parameters are shown in bold and the membrane biophysics properties are shown in regular font. C) Synaptic probabilities. Left: General pipeline for obtaining the connection probabilities, number of contacts, and dendritic and axonal path lengths from 2D reconstructions. Middle: Example of a connectivity diagram of a DG Granule cell and two interneurons

across the different parcels of DG. Probabilities of connection (mean ± SD) are shown in black, numbers of contacts in gray, dendritic path lengths in blue, and axonal lengths in red. Right top: Total number of connections within DG by connection type. Right bottom: Breakdown of the total number of connections by parcel and connection type. D) Synaptic physiology. Left: General pipeline for obtaining normalized synaptic parameters from paired recordings with a TPM model. Right top: Digitized synaptic data between two EC LII-III Pyramidal-Tripolar cells. Experimental data are shown in blue, initiation synaptic points in pink, model data in orange, and corrected data in green. Right bottom: Simulated modeling conditions, electrophysiological parameters, and TPM parameters. Abbreviations by panel: A) PC: Pyramidal cell; BC: Basket cell; WA BC: Wide-Arbor Basket cell; BiC: Bistratified cell; Exc: excitatory; Inh: inhibitory. B) V_r: resting membrane potential; V_t: firing threshold potential; V_{peak}: spike cutoff potential; V_{min}: post-spike reset potential. C) E-E: excitatory-excitatory; E-I: excitatory-inhibitory; I-I: inhibitory-inhibitory; I-E: inhibitory-excitatory. D) V_h: holding potential; τ_r: recovery time constant; τ_f: facilitation time constant; g: conductance; τ_d: deactivation time constant; U: utilization ratio.

Figure 6. Hippocampome.org data provenance. A) The internal web of constituent neuron-type properties (black thin arrows) that ultimately contribute to the instantiation of spiking neural simulations (orange thick arrows). Properties described qualitatively, such as morphological presence of axons in a layer or molecular biomarker expressions, are in black font. Properties described by quantitative values, such as membrane biophysics and neurite lengths, are in red font. Properties with v2.0 updated information, such as connectivity and firing pattern phenotypes, are depicted by blue hexagons, and v1.x information, such as Izhikevich modeling parameter values and neuron-type census values, is visualized by black circles. B) External resources that contribute data to and receive data from Hippocampome.org (the ModelDB logo has been modified from the original).

Figure 7. CARLsim simulation parameters selection and file generation interface. A) The user chooses which subset of the available neuron types to include in the generated downloadable parameter file. Neuron types can be selected (check boxes and gray highlights) either individually or by groupings, such as by subregion and/or by importance rank. B) Representative user selection. C) Downloadable neuron-level parameters. D) Downloadable connection-level parameters.

Figure 8. Hierarchy of neuronal connectivity in Hippocampome.org. A) Subregional connectivity, where the number of connections between subregions is shown, and the node size is proportional to the number of neuron types in each subregion. B) The reciprocal connectivity between DG and CA3 neuron types consists of 147 connections. The node size is proportional to the census size for each neuron type. C) The full connectivity involving DG Granule and CA3 Basket neuron types consists of 98 connections. The node size is proportional to the census size for each neuron type, and the thicknesses of the connecting arrows are proportional to the synaptic probability. The dashed lines are connections for which the synaptic probability has been approximated based on the means of known values. D) The electrophysiological connection between a DG Granule cell and a CA3 Basket cell. The *in vivo* firing rate is shown for the presynaptic neuron. The transfer function between the two neuron types is proportional to the synaptic conductance times the single-exponential decay time constant ($g \cdot \tau_d$; rat, male, P56, 32°C, current clamp). The frequency-current (F-I) curve of the single-compartment Izhikevich model of a CA3 Basket cell was obtained with 10 pA current steps. Inset: Izhikevich model firing pattern of a CA3 Basket cell simulated with 430 pA of current applied for 500 ms (vertical and horizontal scale bars, respectively).

1260 **Figure 9.** Spiking neural network simulations. A) Full-scale CA3 model. (Aa) Neuron type connectivity
1261 schematic. (Ab) Theta (4-12 Hz; top), Gamma (25-100 Hz; middle), and Sharp-Wave Ripple (150-200 Hz;
1262 bottom) filtered local field potentials from 175 ms of the simulation. (Ac) Raster plot of 500 Pyramidal
1263 cells and 50 interneurons of each type (top), and representative voltage traces for each neuron type
1264 (bottom) during the same 175 ms of the simulation in (Ab). B) Spatial representation through grid cell
1265 firing. (Ba) Neuron type connectivity schematic. Bb) Simulated animal trajectory (black) with red dots
1266 indicating the firing of a neuron in those locations. Bc) Raster plot of 50 randomly selected neurons from
1267 each type (top), and representative voltage traces for each neuron type. Abbreviations by panel: A) PC:
1268 Pyramidal cell; BiC: Bistratified cell; QuadD: QuadD-LM cell; AAC: Axo-axonic cell; MFA ORDEN: Mossy
1269 Fiber-Associated ORDEN cell; BC CCK+: cholecystokinin-positive Basket cell. B) SC: Medial Entorhinal
1270 Cortex Layer II Stellate cell; PC: Entorhinal Cortex Layer III Pyramidal cell; MP PC: Entorhinal Cortex Layer
1271 I-II Multipolar Pyramidal cell; AA: Entorhinal Cortex Layer II Axo-axonic; BC: Medial Entorhinal Cortex
1272 Layer II Basket; BC MP: Entorhinal Cortex Layer II Basket-Multipolar Interneuron.

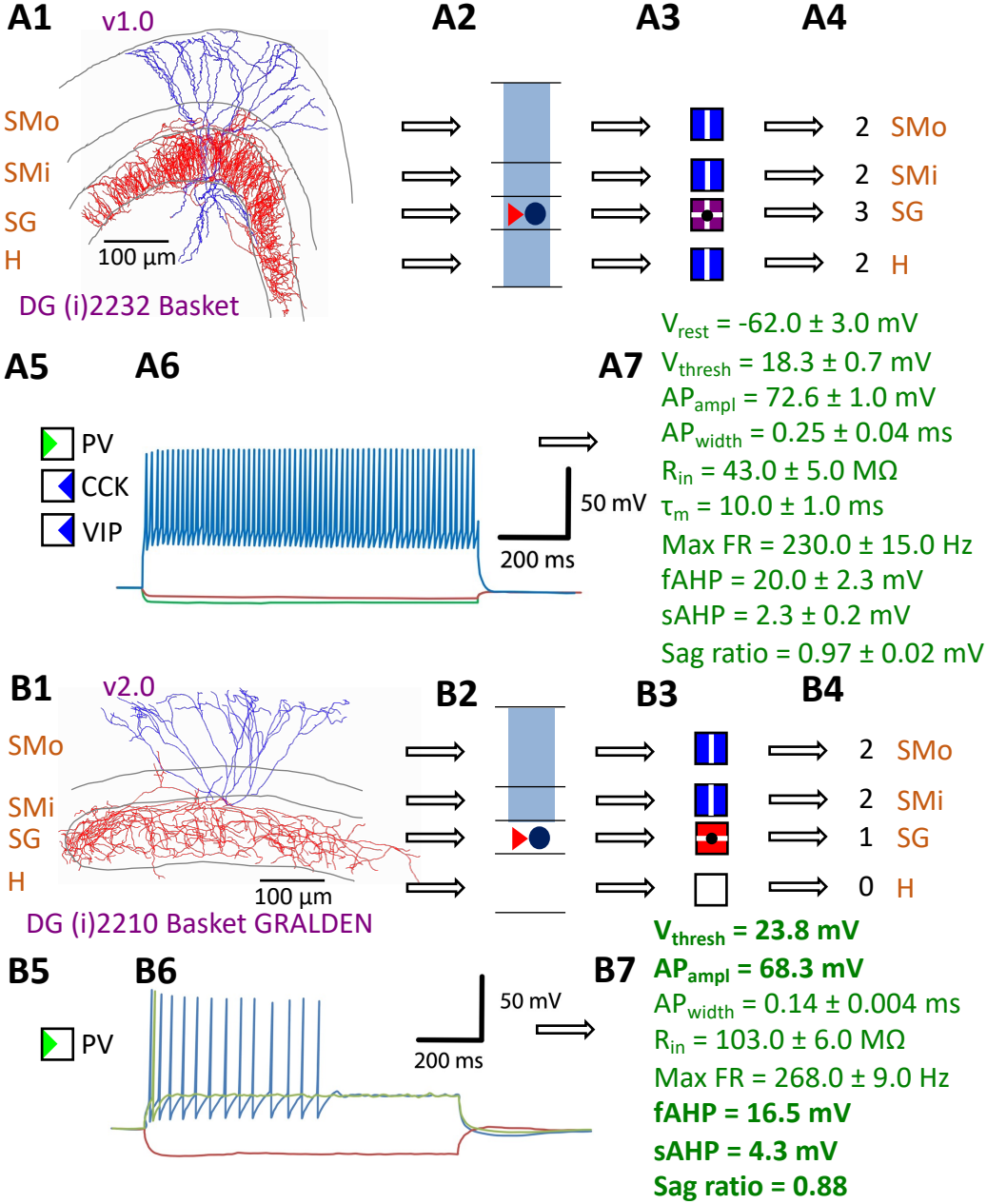
A1
v1.0
SMo
SMi
SG
H
100 µm
DG (i)2232 Basket
A2
A3
A4
2 SMo
2 SMi
3 SG
2 H
A5
A6
A7
PV
CCK
VIP
50 mV
200 ms
V_{rest} = -62.0 ± 3.0 mV
V_{thresh} = 18.3 ± 0.7 mV
AP_{ampl} = 72.6 ± 1.0 mV
AP_{width} = 0.25 ± 0.04 ms
R_{in} = 43.0 ± 5.0 MΩ
τ_m = 10.0 ± 1.0 ms
Max FR = 230.0 ± 15.0 Hz
fAHP = 20.0 ± 2.3 mV
sAHP = 2.3 ± 0.2 mV
Sag ratio = 0.97 ± 0.02 mV
B1
v2.0
SMo
SMi
SG
H
100 µm
DG (i)2210 Basket GRALDEN
B2
B3
B4
2 SMo
2 SMi
1 SG
0 H
B5
B6
B7
PV
50 mV
200 ms
V_{thresh} = 23.8 mV
AP_{ampl} = 68.3 mV
AP_{width} = 0.14 ± 0.004 ms
R_{in} = 103.0 ± 6.0 MΩ
Max FR = 268.0 ± 9.0 Hz
fAHP = 16.5 mV
sAHP = 4.3 mV
Sag ratio = 0.88

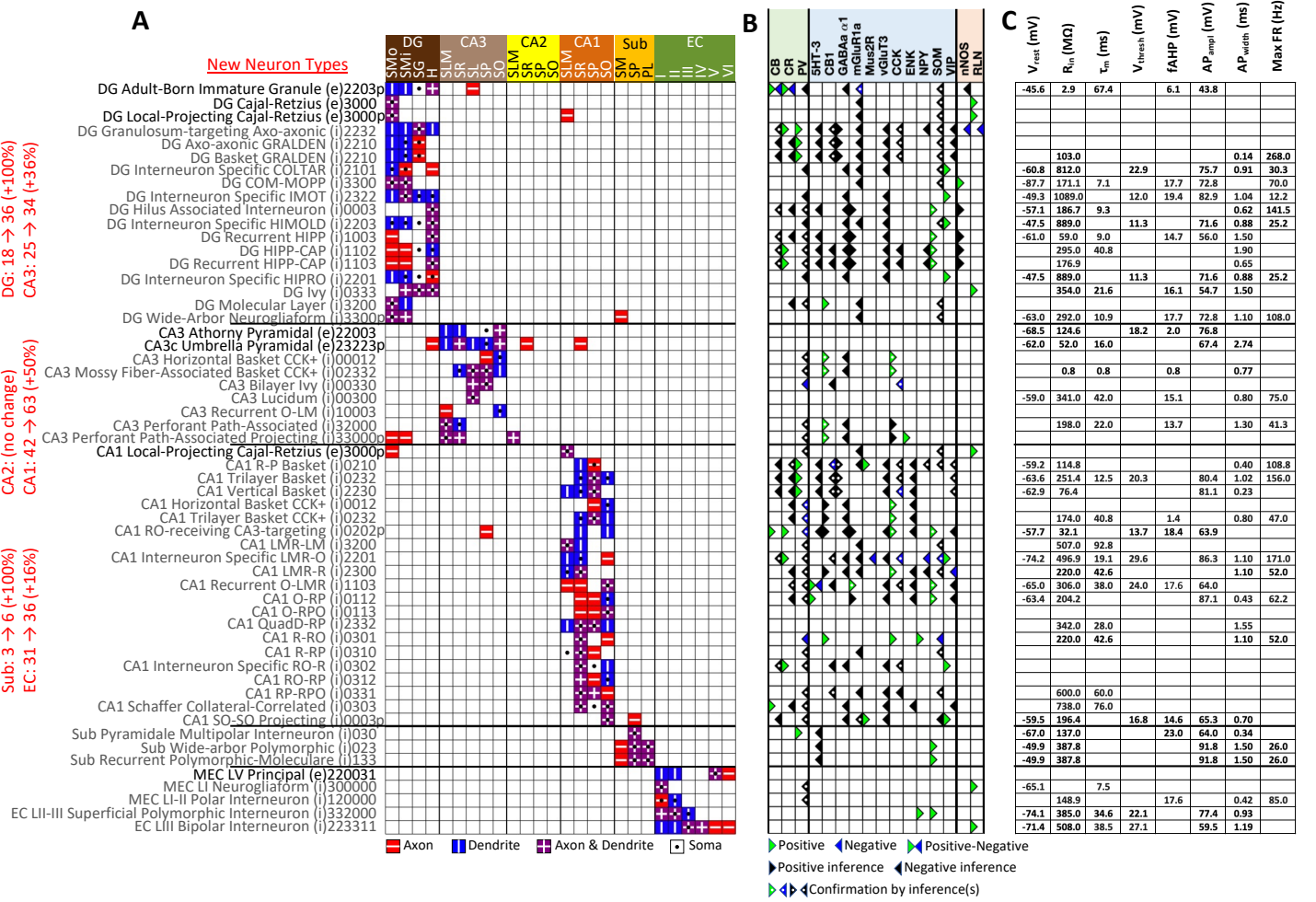
A
New Neuron Types
DG
CA3
CA2
CA1
Sub
EC
SMo SMi SG H SLM SR SL SP SO SLM SR SP SO SLM SR SP SO SM SP PL I II III IV V VI
DG Adult-Born Immature Granule (e)2203p
DG Cajal-Retzius (e)3000
DG Local-Projecting Cajal-Retzius (e)3000p
DG Granulosum-targeting Axo-axonic (i)2232
DG Axo-axonic GRALDEN (i)2210
DG Basket GRALDEN (i)2210
DG Interneuron Specific COLTAR (i)2101
DG COM-MOPP (i)3300
DG Interneuron Specific IMOT (i)2322
DG Hilus Associated Interneuron (i)0003
DG Interneuron Specific HIMOLD (i)2203
DG Recurrent HIPP (i)1003
DG HIPP-CAP (i)1102
DG Recurrent HIPP-CAP (i)1103
DG Interneuron Specific HIPRO (i)2201
DG Ivy (i)0333
DG Molecular Layer (i)3200
DG Wide-Arbor Neurogliaform (i)3300p
CA3 Athorny Pyramidal (e)22003
CA3c Umbrella Pyramidal (e)23223p
CA3 Horizontal Basket CCK+ (i)00012
CA3 Mossy Fiber-Associated Basket CCK+ (i)02332
CA3 Bilayer Ivy (i)00330
CA3 Lucidum (i)00300
CA3 Recurrent O-LM (i)10003
CA3 Perforant Path-Associated (i)32000
CA3 Perforant Path-Associated Projecting (i)33000p
CA1 Local-Projecting Cajal-Retzius (e)3000p
CA1 R-P Basket (i)0210
CA1 Trilayer Basket (i)0232
CA1 Vertical Basket (i)2230
CA1 Horizontal Basket CCK+ (i)0012
CA1 Trilayer Basket CCK+ (i)0232
CA1 RO-receiving CA3-targeting (i)0202p
CA1 LMR-LM (i)3200
CA1 Interneuron Specific LMR-O (i)2201
CA1 LMR-R (i)2300
CA1 Recurrent O-LMR (i)1103
CA1 O-RP (i)0112
CA1 O-RPO (i)0113
CA1 QuadD-RP (i)2332
CA1 R-RO (i)0301
CA1 R-RP (i)0310
CA1 Interneuron Specific RO-R (i)0302
CA1 RO-RP (i)0312
CA1 RP-RPO (i)0331
CA1 Schaffer Collateral-Correlated (i)0303
CA1 SO-SO Projecting (i)0003p
Sub Pyramidale Multipolar Interneuron (i)030
Sub Wide-arbor Polymorphic (i)023
Sub Recurrent Polymorphic-Moleculare (i)133
MEC LV Principal (e)220031
MEC LI Neurogliaform (i)300000
MEC LI-II Polar Interneuron (i)120000
EC LII-III Superficial Polymorphic Interneuron (i)332000
EC LIII Bipolar Interneuron (i)223311
DG: 18 → 36 (+100%)
CA3: 25 → 34 (+36%)
CA2: (no change)
CA1: 42 → 63 (+50%)
Sub: 3 → 6 (+100%)
EC: 31 → 36 (+16%)
Axon
Dendrite
Axon & Dendrite
Soma
B
CB CR PV 5HT-3 CB1 GABAa α1 mGluR1a Mus2R vGluT3 CCK ENK NPY SOM VIP nNOS RLN
Positive
Negative
Positive-Negative
Positive inference
Negative inference
Confirmation by inference(s)
C
V_{rest} (mV) | R_{in} (MΩ) | τ_m (ms) | V_{thresh} (mV) | fAHP (mV) | AP_{ampl} (mV) | AP_{width} (ms) | Max FR (Hz)
-45.6 | 2.9 | 67.4 | | 6.1 | 43.8 | | |
103.0 | | | | | | 0.14 | 268.0
-60.8 | 812.0 | | 22.9 | | 75.7 | 0.91 | 30.3
-87.7 | 171.1 | 7.1 | | 17.7 | 72.8 | | 70.0
-49.3 | 1089.0 | | 12.0 | 19.4 | 82.9 | 1.04 | 12.2
-57.1 | 186.7 | 9.3 | | | | 0.62 | 141.5
-47.5 | 889.0 | | 11.3 | | 71.6 | 0.88 | 25.2
-61.0 | 59.0 | 9.0 | | 14.7 | 56.0 | 1.50 |
295.0 | 40.8 | | | | | 1.90 |
176.9 | | | | | | 0.65 |
-47.5 | 889.0 | | 11.3 | | 71.6 | 0.88 | 25.2
354.0 | 21.6 | | | 16.1 | 54.7 | 1.50 |
-63.0 | 292.0 | 10.9 | | 17.7 | 72.8 | 1.10 | 108.0
-68.5 | 124.6 | | 18.2 | 2.0 | 76.8 | |
-62.0 | 52.0 | 16.0 | | | 67.4 | 2.74 |
0.8 | 0.8 | | | 0.8 | | 0.77 |
-59.0 | 341.0 | 42.0 | | 15.1 | | 0.80 | 75.0
198.0 | 22.0 | | 13.7 | | 1.30 | 41.3
-59.2 | 114.8 | | | | | 0.40 | 108.8
-63.6 | 251.4 | 12.5 | 20.3 | | 80.4 | 1.02 | 156.0
-62.9 | 76.4 | | | | 81.1 | 0.23 |
174.0 | 40.8 | | | 1.4 | | 0.80 | 47.0
-57.7 | 32.1 | | 13.7 | 18.4 | 63.9 |
507.0 | 92.8 | | | | | |
-74.2 | 496.9 | 19.1 | 29.6 | | 86.3 | 1.10 | 171.0
220.0 | 42.6 | | | | | 1.10 | 52.0
-65.0 | 306.0 | 38.0 | 24.0 | 17.6 | 64.0 |
-63.4 | 204.2 | | | | 87.1 | 0.43 | 62.2
342.0 | 28.0 | | | | | 1.55 |
220.0 | 42.6 | | | | | 1.10 | 52.0
600.0 | 60.0 | | | | | |
738.0 | 76.0 | | | | | |
-59.5 | 196.4 | | 16.8 | 14.6 | 65.3 | 0.70 |
-67.0 | 137.0 | | | 23.0 | 64.0 | 0.34 |
-49.9 | 387.8 | | | | 91.8 | 1.50 | 26.0
-49.9 | 387.8 | | | | 91.8 | 1.50 | 26.0
-65.1 | | 7.5 | | | | |
148.9 | | | | 17.6 | | 0.42 | 85.0
-74.1 | 385.0 | 34.6 | 22.1 | | 77.4 | 0.93 |
-71.4 | 508.0 | 38.5 | 27.1 | | 59.5 | 1.19 |

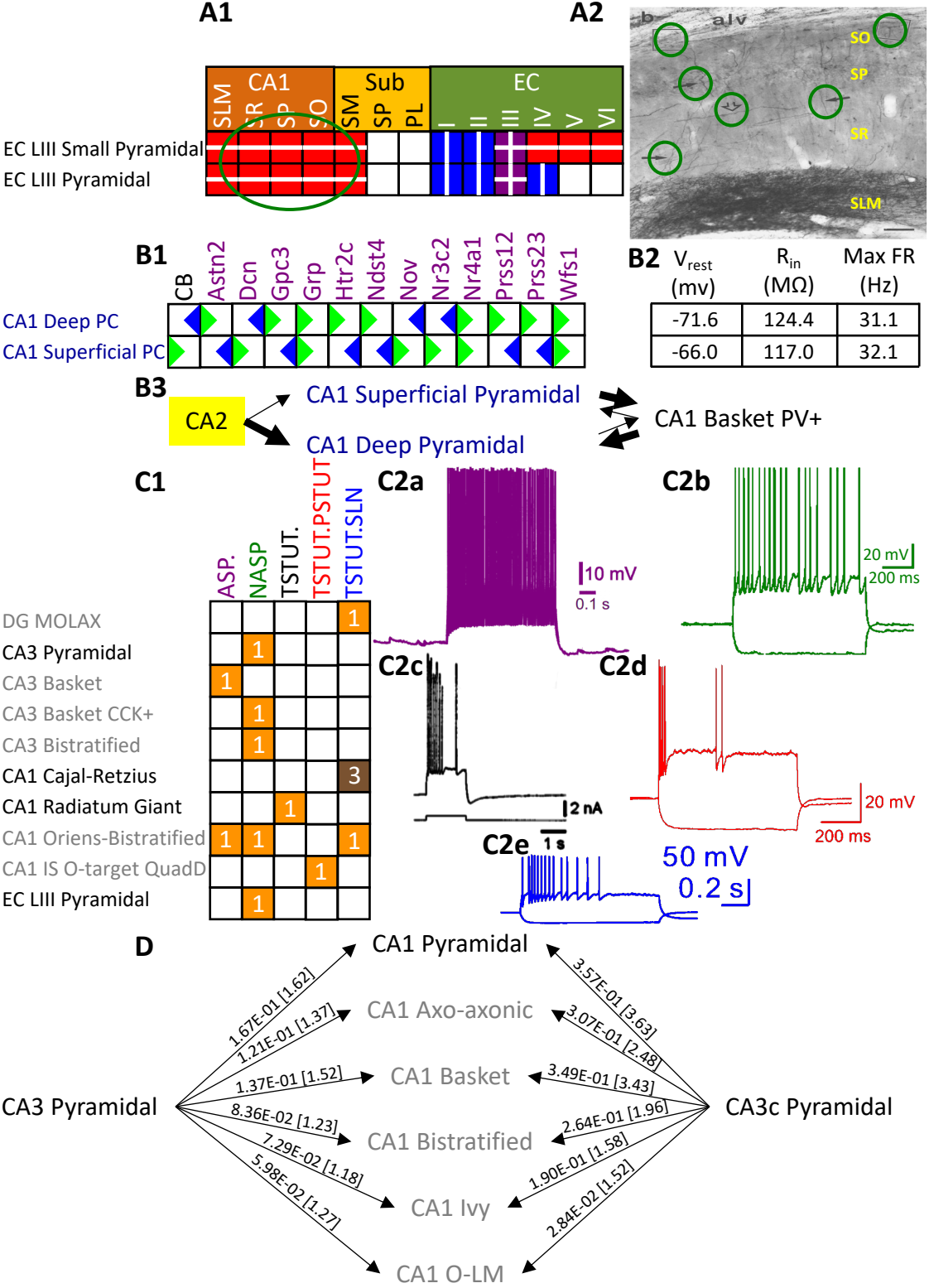
A1
A2
CA1
SLM
SR
SP
SO
Sub
SM
SP
PL
EC
I
II
III
IV
V
VI
EC LIII Small Pyramidal
EC LIII Pyramidal
SO
SP
SR
SLM
B1
CB
Astn2
Dcn
Gpc3
Grp
Htr2c
Ndst4
Nov
Nr3c2
Nr4a1
Prss12
Prss23
Wfs1
CA1 Deep PC
CA1 Superficial PC
B2
Vrest (mv)
Rin (MΩ)
Max FR (Hz)
-71.6 124.4 31.1
-66.0 117.0 32.1
B3
CA2
CA1 Superficial Pyramidal
CA1 Deep Pyramidal
CA1 Basket PV+
C1
ASP.
NASP
TSTUT.
TSTUT.PSTUT
TSTUT.SLN
DG MOLAX
CA3 Pyramidal
CA3 Basket
CA3 Basket CCK+
CA3 Bistratified
CA1 Cajal-Retzius
CA1 Radiatum Giant
CA1 Oriens-Bistratified
CA1 IS O-target QuadD
EC LIII Pyramidal
C2a
10 mV
0.1 s
C2b
20 mV
200 ms
C2c
2 nA
C2d
20 mV
200 ms
C2e
1 s
50 mV
0.2 s
D
CA1 Pyramidal
CA1 Axo-axonic
CA1 Basket
CA1 Bistratified
CA1 Ivy
CA1 O-LM
CA3 Pyramidal
CA3c Pyramidal
1.67E-01 [1.62]
1.21E-01 [1.37]
1.37E-01 [1.52]
8.36E-02 [1.23]
7.29E-02 [1.18]
5.98E-02 [1.27]
3.57E-01 [3.63]
3.07E-01 [2.48]
3.49E-01 [3.43]
2.64E-01 [1.96]
1.90E-01 [1.58]
2.84E-02 [1.52]

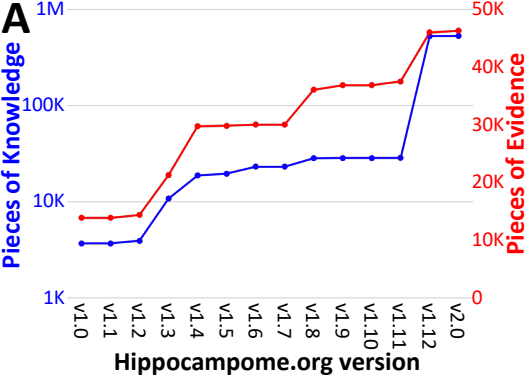
A
Pieces of Knowledge
1M
100K
10K
1K
Pieces of Evidence
50K
40K
30K
20K
10K
0
v1.0
v1.1
v1.2
v1.3
v1.4
v1.5
v1.6
v1.7
v1.8
v1.9
v1.10
v1.11
v1.12
v2.0
Hippocampome.org version

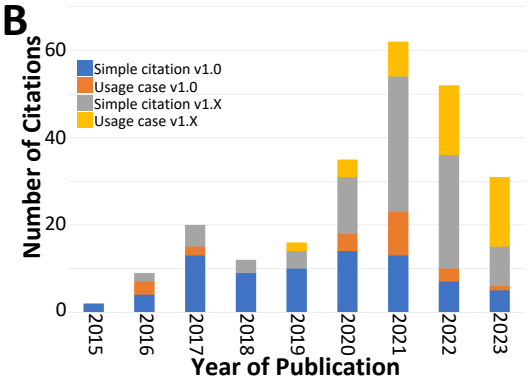
B
Number of Citations
60
40
20
0
Simple citation v1.0
Usage case v1.0
Simple citation v1.X
Usage case v1.X
2015
2016
2017
2018
2019
2020
2021
2022
2023
Year of Publication

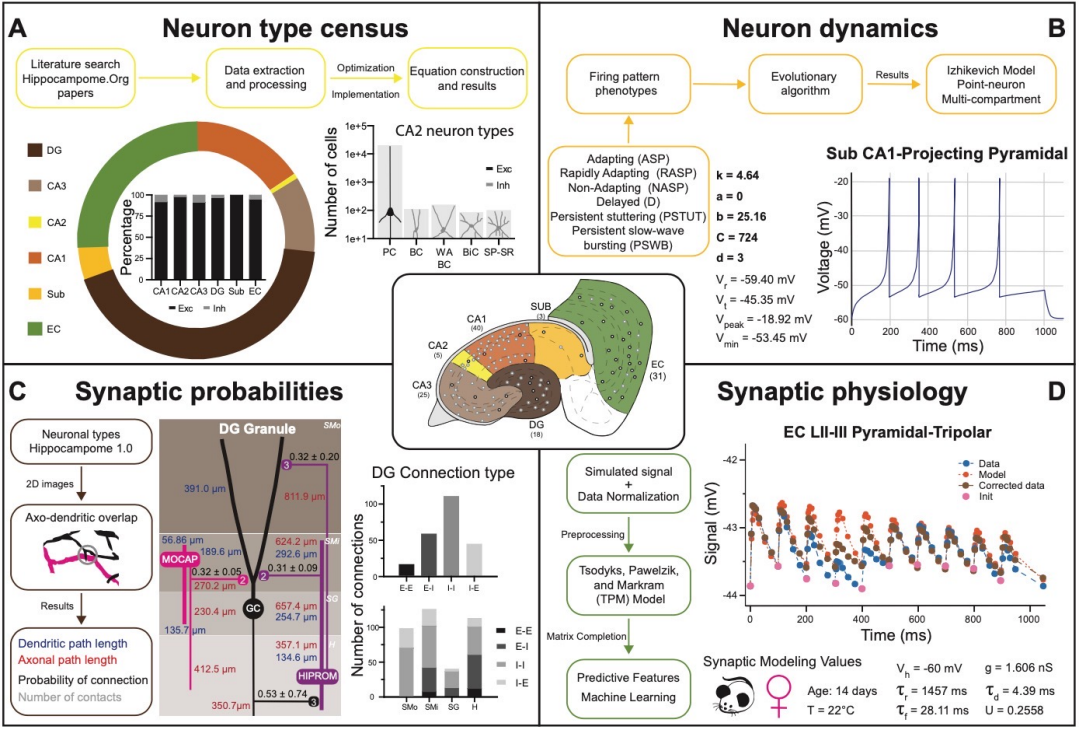
A
Neuron type census
Literature search Hippocampome.Org papers
Data extraction and processing
Optimization
Implementation
Equation construction and results
DG
CA3
CA2
CA1
Sub
EC
Percentage
CA1 CA2 CA3 DG Sub EC
Exc
Inh
CA2 neuron types
Number of cells
PC
BC
WA BC
BiC
SP-SR
B
Neuron dynamics
Firing pattern phenotypes
Evolutionary algorithm
Results
Izhikevich Model Point-neuron Multi-compartment
Adapting (ASP)
Rapidly Adapting (RASP)
Non-Adapting (NASP)
Delayed (D)
Persistent stuttering (PSTUT)
Persistent slow-wave bursting (PSWB)
k = 4.64
a = 0
b = 25.16
C = 724
d = 3
V_r = -59.40 mV
V_t = -45.35 mV
V_{peak} = -18.92 mV
V_{min} = -53.45 mV
Sub CA1-Projecting Pyramidal
Voltage (mV)
Time (ms)
SUB
CA1
CA2
CA3
DG
EC
C
Synaptic probabilities
Neuronal types Hippocampome 1.0
2D images
Axo-dendritic overlap
Results
Dendritic path length
Axonal path length
Probability of connection
Number of contacts
DG Granule
MOCAP
HIPROM
GC
DG Connection type
Number of connections
E-E
E-I
I-I
I-E
SMo
SMi
SG
H
D
Synaptic physiology
Simulated signal + Data Normalization
Preprocessing
Tsodyks, Pawelzik, and Markram (TPM) Model
Matrix Completion
Predictive Features Machine Learning
EC LII-III Pyramidal-Tripolar
Data
Model
Corrected data
Init
Signal (mV)
Time (ms)
Synaptic Modeling Values
Age: 14 days
T = 22°C
V_h = -60 mV
τ_r = 1457 ms
τ_f = 28.11 ms
g = 1.606 nS
τ_d = 4.39 ms
U = 0.2558

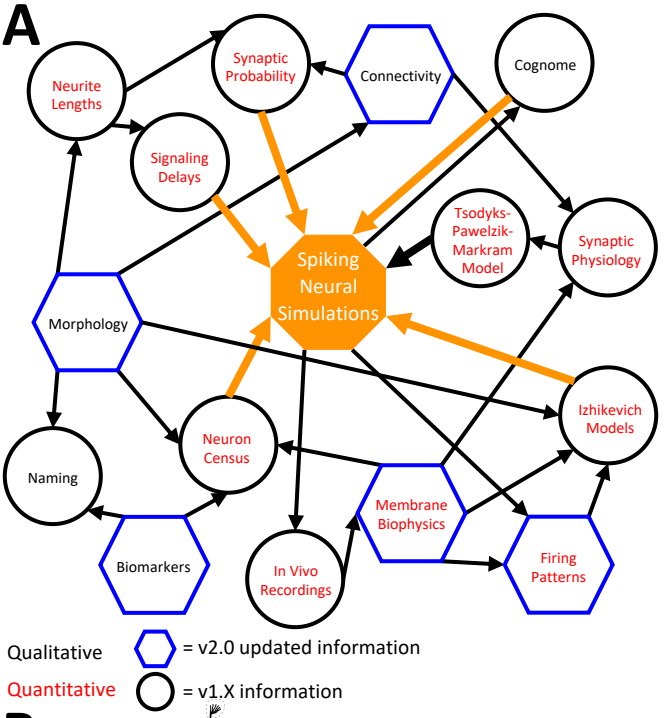
A
Neurite Lengths
Synaptic Probability
Connectivity
Cognome
Signaling Delays
Tsodyks-Pawelzik-Markram Model
Synaptic Physiology
Spiking Neural Simulations
Morphology
Izhikevich Models
Neuron Census
Naming
Membrane Biophysics
Biomarkers
In Vivo Recordings
Firing Patterns
Qualitative
= v2.0 updated information
Quantitative
= v1.X information

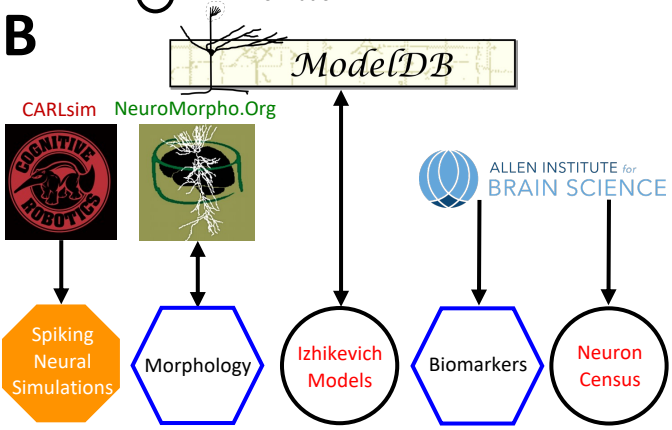
B
ModelDB
CARLsim
NeuroMorpho.Org
ALLEN INSTITUTE for BRAIN SCIENCE
Spiking Neural Simulations
Morphology
Izhikevich Models
Biomarkers
Neuron Census

A

Hippocampome.org

Simulation Parameters Selection

Download a precomputed parameter set zip file:

DG CA3 CA2 CA1

Sub EC All

OR select a user-defined parameter set:

☐ All neuron types

Generate zip file

☐ DG ☐ CA3 ☐ CA2 ☐ CA1 ☐ Sub ☐ EC

☐ All rank 1-5 neuron types

☐ All rank 1-3 neuron types

☐ All canonical neuron types

B

DG (0/35)	CA3 (0/33)	CA2 (3/5)
☐ DG Granule	☐ CA3 Pyramidal	☐ CA2 Pyramidal
☐ DG Semilunar GC	☐ CA3c Pyramidal	☐ CA2 Basket
☐ DG Mossy	☐ CA3 Giant	☐ CA2 Wide-Arbor BC
☐ DG AIPRIM	☐ CA3 Granule	☐ CA2 Bistratified
☐ DG Axo-axonic	☐ CA3 Axo-axonic	☐ CA2 SP-SR

C

Neuron Type	E/I	rank	Population Size	Izh Vr	Izh Vt	Izh a	Izh b	Izh k	Izh d	Izh C
CA2_Pyramidal	e	3	18956	-72.59	-58.78	0.00	-15.89	5.94	74	1630
CA2_Basket	i	3	105	-70.31	-49.91	0.01	-28.48	5.12	132	150
CA2_Bistratified	i	3	79	-74.10	-40.19	0.01	4.75	0.80	4	118

D

Presynaptic	Postsynaptic	TPM g	TPM tau_d	TPM tau_r	TPM tau_f	TPM U	Conn Prob
CA2_Pyramidal	CA2_Pyramidal	2.54	3.42	215.28	102.02	0.29	0.03091
CA2_Basket	CA2_ Pyramidal	3.98	6.25	580.69	10.61	0.27	0.00684
CA2_Bistratified	CA2_ Pyramidal	4.58	5.70	588.65	10.00	0.28	0.08168
CA2_Pyramidal	CA2_ Basket	4.44	2.46	138.68	163.55	0.37	0.03159
CA2_Basket	CA2_Basket	2.78	5.41	508.31	28.25	0.26	0.00423
CA2_Bistratified	CA2_ Basket	3.16	4.93	510.18	27.01	0.26	0.08287
CA2_Pyramidal	CA2_ Bistratified	2.32	2.47	143.16	122.67	0.29	0.04682
CA2_Basket	CA2_ Bistratified	2.06	5.59	504.11	22.74	0.24	0.00423
CA2_Bistratified	CA2_Bistratified	2.29	5.12	508.27	21.67	0.24	0.09951

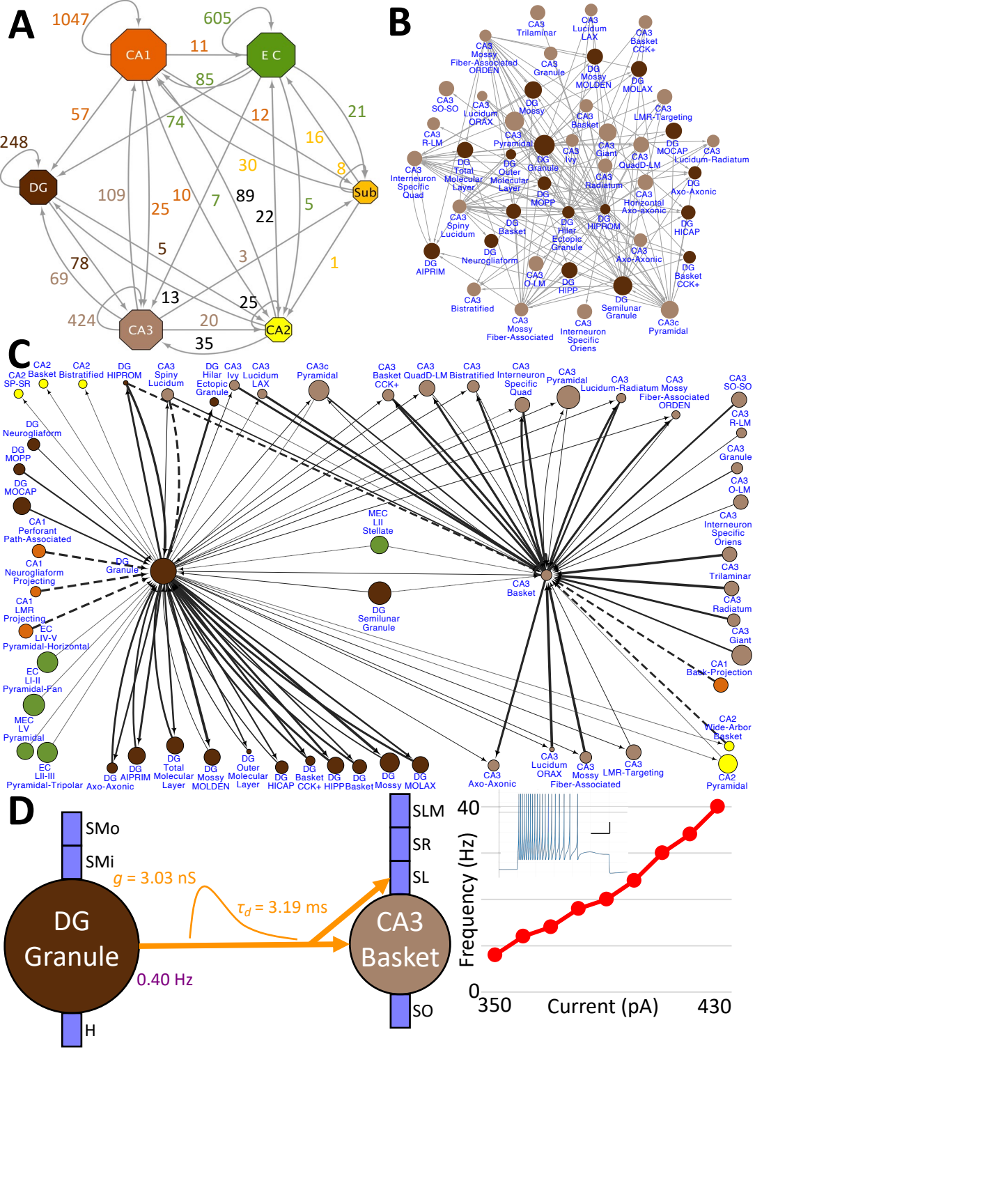
A
CA1
E C
DG
Sub
CA3
CA2
1047
605
11
85
57
74
12
21
248
16
30
8
109
10
7
89
25
22
5
5
3
1
78
69
13
25
424
20
35
B
C
D
SMo
SMi
g = 3.03 nS
τd = 3.19 ms
DG Granule
0.40 Hz
H
SLM
SR
SL
CA3 Basket
SO
40
Frequency (Hz)
0
350
Current (pA)
430

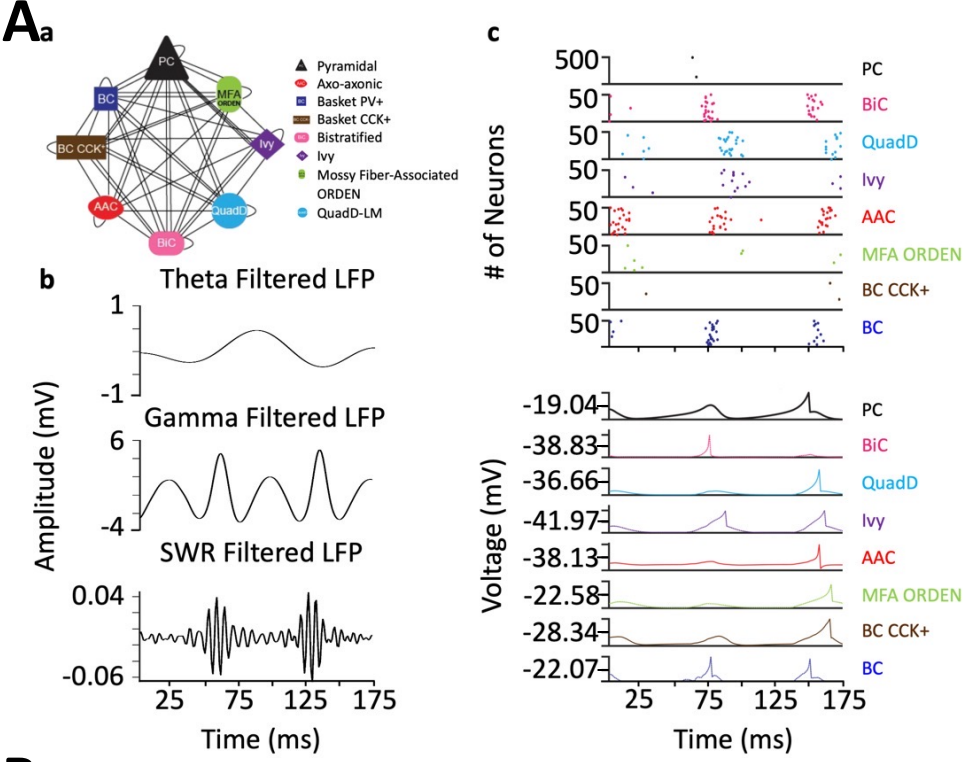
A
a
PC
BC
MFA ORDEN
BC CCK+
Ivy
AAC
QuadD
BiC
Pyramidal
Axo-axonic
Basket PV+
Basket CCK+
Bistratified
Ivy
Mossy Fiber-Associated ORDEN
QuadD-LM
b
Theta Filtered LFP
Gamma Filtered LFP
SWR Filtered LFP
Amplitude (mV)
Time (ms)
c
# of Neurons
PC
BiC
QuadD
Ivy
AAC
MFA ORDEN
BC CCK+
BC
Voltage (mV)
Time (ms)

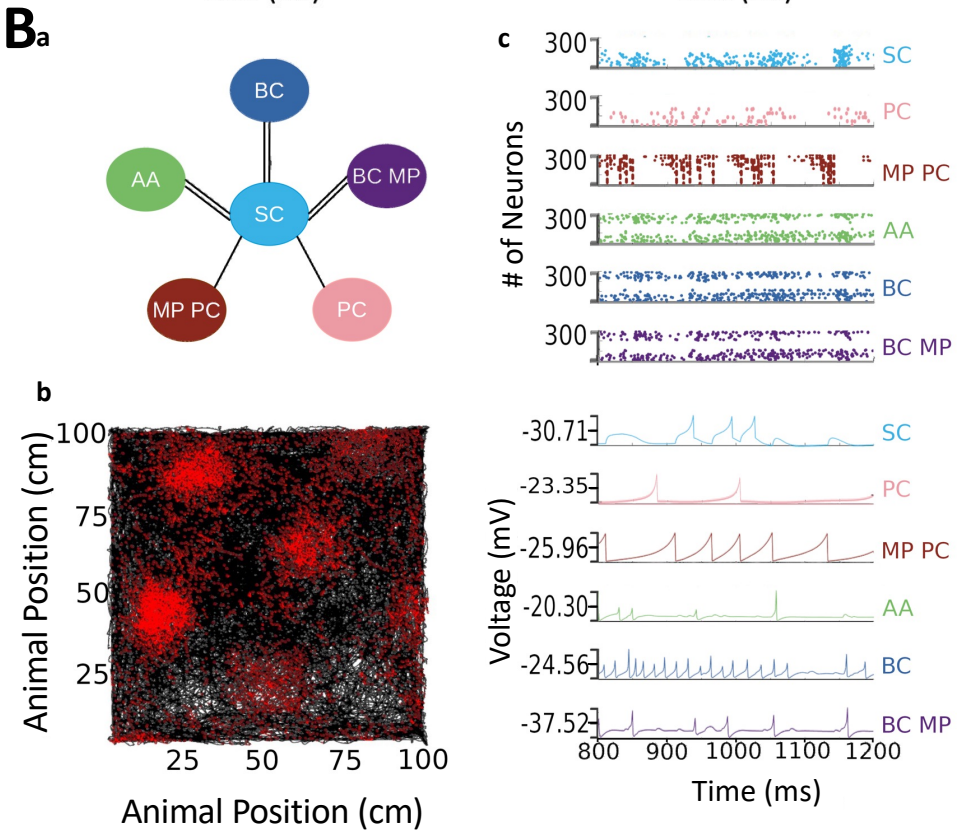
B
a
BC
AA
BC MP
SC
MP PC
PC
b
Animal Position (cm)
Animal Position (cm)
c
# of Neurons
SC
PC
MP PC
AA
BC
BC MP
Voltage (mV)
Time (ms)